Monocyte-derived Dendritic Cells Perform Hemophagocytosis to Fine-tune Excessive Immune Responses

Hideaki Ohyagi[1,10], Nobuyuki Onai[2,3,10], Taku Sato[2,3], Satoshi Yotsumoto[2], Jiajia Liu[1], Hisaya Akiba[4], Hideo Yagita[4], Koji Atarashi[5], Kenya Honda[5], Axel Roers[6], Werner Müller[7], Kazutaka Kurabayashi[2], Mayuka Hosoi-Amaike[2], Naoto Takahashi[1], Makoto Hirokawa[8], Kouji Matsushima[3,9], Kenichi Sawada[1] and Toshiaki Ohteki[2,3]

[1]Department of Hematology, Nephrology and Rheumatology, Akita University Graduate School of Medicine, Akita 010-8543, Japan.

[2]Department of Biodefense Research, Medical Research Institute, Tokyo Medical and Dental University, Tokyo 113-8510, Japan.

[3]Japan Science and Technology Agency, Core Research for Evolutional Science and Technology (CREST), Tokyo 102-0075, Japan.

[4]Department of Immunology, Juntendo University School of Medicine, Tokyo 113-8421, Japan.

[5]Department of Immunology, Graduate School of Medicine, The University of Tokyo, Tokyo 113-0033, Japan.

[6]Institute for Immunology, University of Technology Dresden, Medical Faculty Carl-Gustav Carus, 01307 Dresden, Germany.

[7]Faculty of Life Science, University of Manchester, UK.

[8]Clinical Oncology Center, Akita University Hospital, Akita 010-8543, Japan.

[9]Department of Molecular Preventive Medicine, Graduate School of Medicine, The University of Tokyo, Tokyo 113-0033, Japan

[10]These authors contributed equally to this work

* Correspondence: ohteki.bre@mri.tmd.ac.jp (T.O.)

SUMMARY

Since immune responses simultaneously defend and injure the host, the immune system must be finely regulated to insure the host's survival. Here, we show that when injected with high TLR ligand doses or infected with LCMV clone 13, which has a high viral turnover, inflammatory monocyte-derived dendritic cells (Mo-DCs) are induced to engulf apoptotic erythroid cells. In this process, called hemophagocytosis, extracellular ATP and phosphatidylserine (PS) serve as "find-me" and "eat-me" signals, respectively. Type I IFNs are necessary for both PS exposure on erythroid cells and the expression of PS receptors in the Mo-DCs. Importantly, hemophagocytosis is required for IL-10 production from Mo-DCs. Blocking hemophagocytosis or Mo-DC-derived IL-10 significantly increases CTL activity, tissue damage, and mortality in virus-infected hosts, suggesting that hemophagocytosis moderates immune responses to assure the host's survival *in vivo*. This sheds light on the induction mechanisms and physiological relevance of hemophagocytosis in severe inflammatory and infectious diseases.

INTRODUCTION

An immune response is a two-edged sword that, while directly attacking a pathogen, simultaneously damages the body (Schneider and Ayres,2008). In an infected host, DCs and other innate immune cells sense pathogens through receptors that detect pathogen-associated molecular patterns (PAMPs) or damage-associated molecular patterns (DAMPs). These danger signals trigger DC maturation and induce immunogenic DCs that produce inflammatory cytokines and activate both the innate and adaptive immune systems. The adaptive immune system eliminates the pathogen in an Ag-specific manner and protects the host from re-infection (Medzhitov and Janeway,

1997; Banchereau et al., 2000; Cooper and Alder, 2006). However, infection-induced immune responses, particularly virus-specific CTLs, cytokines, and chemical mediators, simultaneously damage tissue (Clark, 2007; Lambth, 2007; Rouse and Sehrawa, 2010). Therefore, immune responses require regulatory machinery to maintain the fine balance between defense and self-injury during infections; the more severe the infection, the greater the regulatory control must be. However, little attention has been paid to the nature of the machinery balancing these immune-response effects. This study focuses on hemophagocytosis, which is conventionally viewed as an indicator of severe inflammation, and newly identifies DC-mediated hemophagocytosis as the machinery that fine-tunes immune responses and assures host survival under severe inflammatory and infectious conditions.

RESULTS

TLR Ligands Induce Hemophagocytosis

Pattern recognition receptors (PRRs), including Toll-like receptors (TLRs) and NOD-like receptors (NLRs), sense microbial infection and mediate immune and inflammatory responses (Kawai and Akira, 2010). In this study, we found that high doses (~200 μg) of various TLR and NLR ligands injected into wild-type (WT) mice induced hemophagocytosis, an indicator of severe inflammatory conditions such as hemophagocytic syndrome (Larroche and Mouthon, 2003; Janka, 2007; Maakaroun et al., 2010). Hemophagocytosis, typically defined as the engulfment of $TER119^+$ erythroid cells by $CD11c^+$ cells, was detected by the presence of $CD11c^+TER119^+$ cells without permeabilization in the peripheral blood (PB). Of the ligands used, unmethylated CpG DNA (CpG) and poly I:C induced hemophagocytosis in the

peripheral blood (PB) most efficiently (**Figure 1A**). After injecting CpG, the number of $CD11c^+TER119^+$ cells in the PB increased according to the CpG dosage, peaking 18 h later in the bone marrow (BM) and PB and 3 days afterwards in the spleen (**Figures S1A-S1D**). This suggests that hemophagocytosis in the PB correlated well with and reflected that in the BM. Sorted $CD11c^+TER119^+$ cells displayed typical hemophagocytosis with both attached and internalized erythroid cells by Diff-Quick stain and electron microscopic analysis (**Figures 1B and 1C**). CpG also induced other criteria of hemophagocytic syndrome, including fever, splenomegaly, cytopenia (evaluated by the reduction of hemoglobin and platelets), and hypertriglyceridemia (**Figures S1E-S1I**). We used a recently reported protocol (Zoller et al., 2011) to further confirm the intracellular localization of erythroid cells inside $CD11c^+$ cells. In brief, TER119 exposed on $CD11c^+$ cell surfaces was blocked with saturating amounts of an unlabeled Ab against TER119, and then stained with an anti-TER119 Ab. As expected, no $TER119^+$ cells were detected without permeabilization (**Figure S2A**), while intracellular TER119 was stained after permeabilization in a CpG dose-dependent manner (**Figures S2B and S2C**). These results clearly demonstrated the intracellular localization of erythroid cells and correlated well with those of $CD11c^+TER119^+$ staining without permeabilization (**Figures S1D and S2C**). This is reasonable, since hemophagocytosis is a sequential event: apoptotic erythroid cells expressing phosphatidylserine (PS) are initially attached to PS receptors on the $CD11c^+$ cells, and then are gradually phagocytosed into the cells.

Hemophagocytosing DCs Are of Monocyte Origin

The phenotype of the hemophagocytosing $CD11c^+$ cells was MHC class $II^{low}CD11b^{high}F4/80^+Gr\text{-}1^{high}CD40^-CD80^{high}CD86^-$ (**Figure 1D**). This is characteristic of inflammatory monocyte-derived DCs (Mo-DCs), which are induced under inflammatory conditions (Randolph et al., 1999; Leon et al., 2007; Serbina et al., 2008; Auffray et al., 2009; Geissmann et al., 2010). To confirm the Mo-DCs' origin, we sorted inflammatory monocytes, defined as $Ly6c^{high}CX_3CR1^{int}CD11b^+CD11c^-$ cells, from the BM of $Cx_3cr1^{GFP/+}$ mice ($CD45.1^-CD45.2^+$), which express EGFP under the endogenous *Cx3cr1* locus (Jung et al., 2000) (**Figure S3A**). We injected these cells into WT mice ($CD45.1^+CD45.2^-$) and then injected CpG. After 18 h, the transferred inflammatory monocytes had become $CD11c^+$, and approximately 40% were engulfing $TER119^+$ cells (**Figures 1E and 1F**). In $Cx_3cr1^{GFP/+}$ mice injected directly with CpG, the hemophagocytes consisted mostly of $Ly6c^{high}CX_3CR1^{int}$ inflammatory monocyte-derived DCs (**Figure S3B**), indicating that inflammatory monocytes were the major hemophagocyte precursor. During infection and inflammation, inflammatory monocytes mobilize from the BM to the periphery CCR2-dependently (Boring et al., 1997; Serbina et al., 2006). Since CpG-induced hemophagocytosis is mediated by Mo-DCs, we conducted experiments with $Ccr2^{-/-}$ mice, in which circulating monocytes are able to leave the BM but inflammatory monocytes cannot. In WT mice, serum levels of the CCR2 ligands CCL2, CCL7, and CCL12 peaked 3-6 h after CpG injection (**Figures 2A-2C**); CCR2 was predominantly expressed on $Ly6c^{high}$ inflammatory monocytes and to a lesser extent on $CD11c^+TER119^+$ cells (**Figure 2D**). Importantly, the percentage of PB $CD11c^+TER119^+$ cells after CpG injection was greatly reduced in the $Ccr2^{-/-}$ mice (Boring et al., 1997), partially reduced in $Ccl2^{-/-}$ mice (Lu et al., 1998), probably due to CCL7 and CCL12, which are also CCR2 ligands, and unaffected in $Cx_3cr1^{GFP/GFP}$ mice (**Figure 2E**). In contrast, the BM $CD11c^+TER119^+$ cell levels after

CpG injection were comparable between the WT and *Ccr2*$^{-/-}$ mice (**Figure 2F**). Collectively, these results demonstrate that CpG injection caused inflammatory monocytes to mobilize to the periphery, differentiate into Mo-DCs, and engulf mainly erythroid cells.

Involvement of "Find Me" and "Eat Me" Signals in TLR Ligand-Induced Hemophagocytosis

Cells undergoing apoptosis release "find me" signals to recruit phagocytes, and expose PS, which is recognized by phagocytes as an "eat me" signal, on their surface (Nagata et al., 2010; Martin et al., 1996). PS is recognized directly by Tim-1 and -4 and indirectly by the $\alpha_V\beta_3$ and $\alpha_V\beta_5$ integrins through milk fat globule EGF factor 8 (MFG-E8), and by TAM family members through Gas6 and protein S (Martin et al, 1996; Hanayama et al., 2002; Kobayashi et al., 2007; Miyanishi et al., 2007; Nakayama et al., 2009). We next examined the roles of "find me" and "eat me" signals in CpG-induced hemophagocytosis. Serum levels of ATP, recently identified as a "find me" signal (Elliott et al., 2009), increased rapidly after CpG injection, peaking 6 h later (**Figure 3A**). The ATP receptor P2Y2 was predominantly expressed on Ly6c^{high} inflammatory monocytes, on BMDCs, and on Mo-DCs performing hemophagocytosis (CD11c$^+$TER119$^+$), but not on T or B cells (**Figure 3B**), suggesting that ATP is an important "find me" signal in hemophagocytosis. Indeed, injecting suramin, a competitive inhibitor of ATP-P2Y2 binding, effectively blocked the CpG-induced hemophagocytosis (**Figure 3C**).

Next, we examined the role of the "eat me" signal in CpG-induced hemophagocytosis. The number of apoptotic erythroid cells expressing PS, defined as annexin V$^+$TER119$^+$

cells, peaked 2-4 h after CpG injection (**Figure 3D**). In this context, most of the apoptotic cells were TER119^{+} erythroid cells, and some apoptotic Gr-1^{high}Ly6c^{+} granulocytes were also detected (**Figures S4A-S4C**). CpG-induced Mo-DCs were the major phagocytes for TER119^{+} erythroid cells (**Figures S5A-S5D**). As “eat me” signal receptors, the Mo-DCs expressed Tim1, Tim4, and α_V and β_3 integrin (**Figure 3E**) and an injection of neutralizing Abs against “eat me” signal receptors significantly blocked hemophagocytosis (**Figure 3F**). CpG injection induced the production of the representative regulatory cytokine IL-10 in the PB at rates that increased with CpG dosage (**Figure 3G**), and this correlated well with hemophagocytosis (**Figures S1D and S2C**). Consistent with these results, excessive CpG stimulation triggers DC IL-10 production (Waibler et al., 2008). Of note, injecting PS receptor-neutralizing Abs, which prevents hemophagocytosis, significantly reduced the IL-10 production (**Figures 3G**). Collectively, these results suggest that “find me” and “eat me” signals are critical for CpG-induced hemophagocytosis, and that high CpG doses induce IL-10 production.

Injecting a high dose of poly I:C into WT mice produced similar results, with Mo-DCs (**Figure S6A**) and “find me” and “eat me” signals (**Figures S6B and S6C**) playing critical roles in the poly I:C-induced hemophagocytosis and accompanying IL-10 production (**Figures S6D and S6E**).

Type I IFN Signaling Is Essential in Virus-Induced Hemophagocytosis

Based on these findings, we examined the induction mechanism and physiological relevance of hemophagocytosis in virus infection. We used the lymphocytic choriomeningitis virus (LCMV) variant clone 13 (C13), which elicits a chronic infection (Matloubian et al., 1990), for two reasons. First, compared with the original LCMV

Armstrong (Arm), C13 binds and infects DCs with high affinity, and it proliferates vigorously owing to two amino acid changes in its glycoprotein and polymerase, resulting in remarkably high viral nucleic acid levels *in vivo* (Sevilla et al., 2010), possibly mimicking the effect of high-dose CpG or poly I:C injection. In this context, we expected that the more severe the infection, the more closely regulated the response. Second, most viruses that induce hemophagocytosis produce a chronic infection in humans (Clark 2007; Lambth 2007; Rouse and Sehrawa, 2010), although the role of hemophagocytosis in chronic infection is unknown. Indeed, the mRNA levels for viral glycoprotein (GP) and nucleoprotein (NP) in C13-infected cells were remarkably higher than in Arm-infected cells, and we newly found that inflammatory monocytes, which are Mo-DC precursors, were a major C13 infection target (**Figure S7A**). As expected from these results, hemophagocytosis was induced more efficiently in C13-infected WT mice than in Arm-infected WT mice (**Figures S7C and S7D**); the intracellular localization of erythroid cells was again confirmed using the Diff-Quick staining and recently reported protocol (Zoller et al., 2011) (**Figures S7B, S7E, and S7F**). As with CpG injection, most of the apoptotic cells were $TER119^{+}$ erythroid cells and some were apoptotic $Gr\text{-}1^{high}Ly6c^{+}$ granulocytes, suggesting that the contribution of apoptotic granulocytes was not negligible but relatively low (**Figures S8A-S8C**). Indeed, we sometimes observed the phagocytosis of granulocytes by Mo-DCs isolated from the PB of C13-infected WT mice (**Figure S8D**). In contrast, lymphocyte populations, including T, B, and NK cells, rarely became apoptotic at the same time point after C13 infection.

C13 infection induced type I IFN production (**Figures 4A and 4B**). Interestingly, C13 infection-induced hemophagocytosis was significantly reduced in mice deficient for IFNAR1, a component of the type I IFN-receptor (**Figures 4C and 4D**). Consistent with these results, C13 infection in *Ifnar*$1^{-/-}$ mice severely impaired the PS exposure on

erythroid cells and the Tim-1, Tim-4, and α_V and β_3 integrin expression on Mo-DCs (**Figures 4E-4G**), suggesting that type I IFNs are essential both for inducing PS on erythroid cells and for the development of Mo-DCs that express PS receptors. Indeed, *ex vivo* IFN-α stimulation directly induced the apoptosis of $TER119^+$ erythroid cells and, to a lesser extent, $Gr\text{-}1^{high}Ly6c^+$ granulocytes (**Figure S9A**). In addition, IFN-α stimulation directly induced expression of PS receptors, i.e. Tim-1, Tim-4, and α_V and β_3 integrin, on inflammatory monocytes, precursors of Mo-DCs (**Figures S9B and S9C**).

Hemophagocytes are the major source of IL-10

Finally, we examined the physiological relevance of hemophagocytosis in C13 infection. As expected from our findings thus far, injecting neutralizing Abs against Tim-1, Tim-4, α_V, and β_3 into C13-infected WT mice significantly suppressed hemophagocytosis (**Figure 5A**). Milk fat globule-epidermal growth factor 8 (MFG-E8) contains a PS-binding domain and an arginine-glycine-aspartate (RGD) motif, which binds to both $\alpha_v\beta_3$ and $\alpha_v\beta_5$ integrin on phagocytic cells, and it mediates the integrin-dependent engulfment of apoptotic cells and subsequent signaling (Hanayama et al., 2002; Akakura et al., 2003). As expected, *Mfge8* was clearly expressed in both inflammatory monocytes, a precursor of Mo-DCs, and Mo-DCs performing hemophagocytosis, whereas expression of other PS receptors including *Bai1*, *Stab2*, *Tyro3*, *Axl*, *Mertk*, *Gas6* detected by qPCR (**Figure S10A**) and Stabilin-2, Tyro-3, Axl, MerTK by specific Ab staining (**Figure S10B**) was minimal, suggesting that these molecules are unlikely involved in the uptake of apoptotic erythroid cells by Mo-DCs. Serum levels of IL-10 and TGF-β1, both of which suppress immune responses, increased after C13 infection,

peaking at 24 h (**Figure 5B** and data not shown). In line with our findings, C13 infection induces IL-10, contributing to the virus persistence *in vivo* (Brooks et al., 2006), although the mechanism of IL-10 production remains unknown. Importantly, injecting Abs against the Mo-DC PS receptor, which block hemophagocytosis, effectively reduced the IL-10 and TGF-β1 production (**Figure 5B**), whereas injecting IL-10-neutralizing Abs into WT mice did not suppress hemophagocytosis (**Figure 5A**). This suggests that the IL-10 production from Mo-DCs in response to C13 infection is hemophagocytosis-dependent. Of note, ERK and p38 phosphorylations, which are prerequisite for IL-10 production, were detected in hemophagocytosing Mo-DCs (**Figures S11A and S11B**). In this context, blocking IL-10 activity substantially reduced the TGF-β1 serum levels, implying that IL-10 somehow regulates TGF-β1 production in C13-infected WT mice (**Figure 5B**). In the PB of C13-infected *Il10*^{Venus} reporter mice (Atarashi et al., 2011), IL-10 was expressed predominantly in CD11c^{+}TER119^{+} cells and not in T cells (**Figure 5C**), and the absolute number of IL-10^{venus+} CD11c^{+}TER119^{+} cells was much greater than that of IL-10^{venus+} cells belonging to other populations, including CD11c^{+}TER119^{-} cells (**Figure 5D**). This clearly demonstrates that hemophagocytes are the major source of IL-10 at an early phase of infection *in vivo*.

To further examine the IL-10 production machinery from Mo-DCs in response to C13 infection, we newly established *ex vivo* hemophagocytosis assay system, in which TER119^{-} Mo-DCs and TER119^{+} erythroid cells, separately sorted from the BM of C13 inefected WT mice, were co-cultured (**Figure 6A**). Of note, the erythroid cells were pHrodo-labelled prior to the co-culture, which allowed the erythroid cells transported into lysosomes upon hemophagocytosis to be detected by their increased light emission under the acidic conditions. Consistent with the *in vivo* results, hemophagocytosis was clearly induced *ex vivo* (**Figures 6A, left panel, 6B, and 6C**). Most importantly, *ex vivo*

blockage of hemophagocytosis with Abs against the Mo-DC's PS receptor impaired Mo-DC-derived IL-10 production (**Figures 6A, right panel, 6D**, **and 6E**). In this context, adding blocking Abs against Tim-1 and Tim-4 did not affect IL-10 production, whereas blocking Abs against integrin α_v, β_3, or $\alpha_v\beta_5$ significantly reduced the level of IL-10 production (**Figure 6E**). In addition, neither blocking internalization of apoptotic erythroid cells with cytochalasin D nor opsonization of them induced Mo-DC-derived IL-10 production (**Figure 6E**). These results collectively demonstrated that IL-10 production from Mo-DCs is largely dependent on the integrin-mediated signals. Similar results were obtained from the co-culture in which Mo-DCs and granulocytes, the other apoptotic population in C13-infected mice (**Figure S8A** and **S8B**), were used in the same experiment (**Figure S12**). Notably, the amounts of IL-10 secreted from the Mo-DCs that engulfed erythroid cells were 60 pg/ml, and from those that engulfed granulocytes were 40 pg/ml in the same experiment (**Figure 6E and S12**). These results suggested that granulocytes are slightly less potent on a per cell basis than erythroid cells for inducing IL-10 secretion from Mo-DCs. To definitively show the contribution of these integrins to the IL-10 secretion from Mo-DCs, we performed *ex vivo* hemophagocytosis assay, in which Mo-DCs and erythroid cells, sorted separately from the BM of WT and *Mfge8*$^{-/-}$ mice after C13 infection, were co-cultured in all combinations (**Figure 6F**). Importantly, the IL-10 secretion was selectively impaired when *Mfge8*$^{-/-}$Mo-DCs were used for the co-culture, demonstrating that the IL-10 secretion from Mo-DCs is MFG-E8-mediated, and thus dependent on both integrin $\alpha_v\beta_3$ and $\alpha_v\beta_5$ (**Figure 6F**).

We also examined the apoptotic status of these cells during later time points, i.e. 8, 16, 24 days after the infection. The numbers of apoptotic erythroid cells were much reduced and comparable to those of granulocytes (**Figure S13A**), implying the equal

contribution of erythroid cells and granulocytes to phagocytosis-mediated IL-10 production, although the numbers of IL-10 producing cells were substantially lower, compared with that at an early phase of infection (**Figure S13B**). As observed at an early phase of infection, lymphocyte populations, i.e. T and B cells, hardly became apoptotic during later time points (**Figure S13A**).

Hemophagocytosis Prevents Immune Responses-Mediated Damage and Assure the Host's Survival

What is the physiological relevance of the hemophagocyte-derived IL-10 in viral infection? Interestingly, blocking hemophagocytosis with PS receptor Abs or IL-10 activity with IL-10 neutralizing Ab enhanced the virus-specific CTL induction (**Figures S14A and S14B**), CTL-mediated liver-damage (Zinkernegel et al., 1986) (serum AST and ALT) (**Figures S14C, and S15A-S15D**), and mortality (**Figure S14D**). In the context of CTL activity, we also found that blocking hemophagocytosis or IL-10 activity diminished the CTL expression of PD-1 (**Figure S14E**), which causes CTL exhaustion in C13 infection (Barber et al., 2006). As Tim-1/Tim-4-signaling may alter immune responses in some cases (Xiao et al., 2007, 2011; Rodriguez-Manzanet et al., 2008), we examined whether anti-Tim-1 and -4 Abs could modulate immune responses in C13-infected WT mice. However, injecting anti-Tim-1 and -4 Abs did not alter the frequency of hemophagocytosis in the PB, IL-10 level and C13 virus titers in the sera, and percentage and absolute number of IL-10^{venus+} CD11c^{+}TER119^{+} cells (**Figures S16A-S16E**), suggesting that these Abs do not significantly affect virus-specific immune responses *in vivo*, at least in this experimental setting.

To further confirm the importance of the hemophagocyte-derived IL-10 in fine-tuning excessive immune responses *in vivo*, *Cd11c*-Cre/*Il10*$^{fl/fl}$ (CKO) mice, in which the hemophagocytes cannot produce IL-10, were infected with C13. While the hemophagocytosis levels in C13-infected CKO mice were comparable to those seen in control WT mice (**Figure 7A**), the serum IL-10 production was greatly reduced (**Figure 7B**), confirming that hemophagocytes are the major source of IL-10 *in vivo* under these infectious conditions. As with WT mice in which hemophagocytosis was blocked, the CKO mice showed excessive CTL activity, tissue damage, and mortality when infected with C13 (**Figures 7C-F**). Taken together, these results point to hemophagocytosis as a novel machinery for preventing excessive immune response-mediated damage, thus assuring the host's survival in the face of severe viral infection.

DISCUSSION

Our findings indicate that hemophagocytosis induced by TLR ligands or viruses occurs in sequential steps (**Figure S17**). We found that hemophagocytosis could be detected by staining with and without permeabilization. In this context, we would like to stress that hemophagocytosis is a sequential event; that is, apoptotic erythroid cells exposing PS are initially attached to PS receptors expressed on the Mo-DCs, and are then gradually phagocytosed into the cells. Therefore, even without permeabilization, these cells can be detected as CD11c^{+}TER119^{+} cells. Supporting the specific recognition of apoptotic erythroid cells by PS receptors on Mo-DCs, hemophagocytosis detected without permeabilization was significantly reduced in WT mice in which hemophagocytosis was blocked with anti-PS receptor Abs or with suramin, a competitive inhibitor of ATP-P2Y2 binding. In C13-infected *Ifnar*1$^{-/-}$ mice, both PS exposure on erythroid cells

and PS receptor induction on Mo-DCs were impaired, suggesting that type I IFNs are critically involved in these processes. As it is well known that CpG injection induces type I IFN production, it is likely that CpG-induced type I IFNs induce apoptosis of erythroid cells. Indeed, *ex vivo* IFN-α stimulation directly induced apoptosis of erythroid cells **(Figure S9A)**. F4/80^{+} macrophages are reported to be the hemophagocytosis-performing cells in the spleen of mice infused with IFN-γ (Zoller et al., 2011). In this context, we found that the hemophagocytosis-performing Mo-DCs clearly expressed F4/80 (**Figure 1D**), suggesting that the previously reported F4/80^{+} macrophages and the Mo-DCs are presumably overlapping populations (Domínguez and Ardavín, 2010).

The uptake of experimentally (UV-irradiation, staurosporine, etc.) induced apoptotic peripheral blood lymphocytes, neutrophils, and peripheral blood T cells or Jurkat T cells by phagocytes induces IL-10 production, which suppresses proinflammatory cytokine production (Voll et al., 1997; Byrne and Reen, 2002; Kim et al., 2004). However, it remains unknown whether such *ex vivo* observations are consistent with and represent the *in vivo* situation under severe inflammatory conditions. Remarkably, we showed that, upon CpG injection or LCMV C13 infection, most of the apoptotic cells were erythroid cells, and a small number were granulocytes (**Figure S4 and S8**). As a result, Mo-DCs preferentially engulfed apoptotic erythroid cells, leading to IL-10 production. Given these findings, we do not exclude the contribution of granulocytes, although it is relatively minor, to the IL-10 secretion from Mo-DCs. Consistent with our findings, the type I IFN-dependent apoptosis of erythroid cells, but not of neutrophils or monocytes, is observed in DNase II deficient mice (Kawane et al., 2001; Yoshida et al., 2005). These results suggested that type I IFN signaling is required for the recruitment of nucleated erythroid cells to the PB and that, compared with other hematopoietic cells,

erythroid cells are relatively sensitive to type I IFN signaling and therefore become apoptotic. Indeed, IFN-α induces apoptosis in human erythroid cells (Tarumi et al., 1995). Notably, these phenotypes observed in DNase II deficient mice are consistent with those in WT mice injected with CpG or infected with C13.

Although hemophagocytosis is viewed as an indicator of hemophagocytic syndrome and other severe inflammatory conditions (Clark 2007; Lambth 2007; Rouse and Sehrawa, 2010), our findings suggest that it rather represents a possible biomarker of anti-inflammatory responses in the host. Very recently, it was reported that repeatedly injecting CpG induces hemophagocytic syndrome-like or macrophage activation syndrome-like disease in mice (Behrens et al., 2011). When IL-10 signaling is blocked in this model, a more severe disease with larger numbers of hemophagocytosis develops, raising two possibilities; first, hemophagocytosis contributes to the severity of the disease, and second, it is induced, as a negative feed-back machinery, to suppress severe inflammatory responses. We propose here that hemophagocytosis is prerequisite for IL-10 production, and that IL-10 is secreted by Mo-DCs in a manner dependent on hemophagocytosis, leading to anti-inflammatory effects of IL-10 to fine-tune immune responses. In humans, hemoglobin uptake by $CD163^+$ macrophages induces the expression of the anti-inflammatory heme oxygenase (HO-1) *ex vivo* (Schaer et al., 2006), and HO-1 expression is detected in hemophagocytic $CD163^+$ macrophages in the BM of patients with fatal sepsis (Schaer et al., 2006). Interestingly, CD163 expression is inducible by IL-10, implying that this anti-inflammatory pathway might also contribute to the prevention of immune responses *in vivo*.

In acute infections, pathogen growth correlates well with indicators of deteriorating health, and inducing immune responses usually restores health by reducing the pathogen

load. However, our findings show that, during severe viral infections, immune responses unaccompanied by efficient hemophagocytosis-mediated fine-tuning lead to a further deterioration in health and eventually to severe immune response-mediated self-damage, despite the virus being effectively eradicated. Of interest, aberrant immune activation with impaired IFN-α expression, a possible cause of limited hemophagocytosis, was evident in macaques infected with the 1918 Spanish pandemic virus (Kobasa et al., 2007).

The more severe the infection, the stronger the immune response must be. The stronger the immune response, the greater the regulatory control must be. Given that most viruses that cause hemophagocytosis, including Epstein-Barr virus, cytomegalovirus, and HIV (Larroche and Mouthon, 2003; Janka, 2007; Maakaroun et al., 2010), establish chronic infections in humans (Clerici et al., 1996; Nordoy et al., 2000; Budiani et al., 2002), the induction of hemophagocytosis may allow the virus to persist in the host, assuring host survival by preventing immune response-mediated damage. Considering this novel trade-off between host and pathogen, our findings may be valuable not only in extending our understanding of immune biology, but also in identifying therapeutic targets for severe inflammatory diseases.

EXPERIMENTAL PROCEDURES

Mice

C57BL/6J (B6, Clea), B6.*Cx$_3$cr1*$^{GFP/+}$ (Jackson) (Jung et al., 2000), B6.*Ccr2*$^{-/-}$ (Jackson) (Boring et al., 1997), B6.*Ccl2*$^{-/-}$ (Lu et al., 1998), B6.*Ifnar1*$^{-/-}$ (B&K Universal), B6.*Il-10*^{Venus} (Atarashi et al., 2011), B6.*Cd11c*-Cre (Jackson) (Strabges et al., 2007), B6.*Mfge8*$^{-/-}$ (Hanayama et al., 2004), and B6.*Il10*$^{fl/fl}$ (Roers et al., 2004) mice were maintained in our SPF facility. All animal experiments were approved by the Institutional Animal Care Committees of Akita University and Tokyo Medical and Dental University.

Reagents and *In Vivo* Injection

LPS, MDP, and cytochalasin D were purchased from Sigma-Aldrich. Other reagents were obtained as follows: poly I:C (GE Healthcare), R848 (Invivogen), CpG (ODN-1668 [5'-TCCATGACGTTCCTGATGCT-3']; Hokkaido System Science), iE-DAP (Invivogen), and recombinant mouse interferon-α (Dainion Sumitomo Pharma Co. Ltd.). Mice were intravenously (i.v.) injected with TLR ligands (200 μg poly I:C, 100 μg LPS, 100 μg R848, or 200 μg CpG) or Nod ligands (100 μg iE-DAP or 100 μg MDP). Mice were infected by i.v. injection of viruses (2 x 10^6 pfu LCMV Armstrong or Clone 13).

Diff-Quick Stain

CD11c$^+$TER119$^+$ cells were sorted from the BM of CpG injected or LCMV C13 infected mice, cytospun at 500 *g* for 5 minutes onto a slide glass, and stained with Diff-Quick (Sysmex).

Electron Microscopy

$CD11c^{+}TER119^{+}$ cells were sorted from the PB of CpG injected mice, fixed with 2.5 % glutaraldehyde in 0.1 M phosphate buffer pH 7.2, washed overnight at 4 °C in the same buffer, and postfixed with 1% OsO_4 at 4 °C for 2 h. Then, the cells were dehydrated in a graded in a series of ethanol and embedded in Epon 812. Ultrathin (1μm) sections were collected on copper grids and with uranyl acetate and lead citrate and then examined by transmission electron microscope, H-7100 (Hitachi).

Hemophagocytosis Blocking

To block ATP activity, 6 mg suramin was intraperitoneally (i.p.) injected into WT mice 30 min after CpG or poly I:C injection, or 3 and 6 days after C13 infection. To block "eat me" signal receptors, WT mice received either 500 μg rat IgG (control) or 500 μg anti-Tim-1 mAb (RMT1-10) (Nakayama et al, 2009), 500 μg anti-Tim-4 mAb (RMT4-54) (Nakayama et al, 2009), 500 μg anti-α_V mAb (RMV-7) (Takahashi et al, 1990), or 500 μg anti-β_3 mAb (HMβ3-1) (Yashuda et al., 1995), or isotype control Ab cocktails including rat IgG2a, rat IgG2c, and hamster IgG (500 μg of each) by i.v., singly or in combination as indicated, 60 min and 120 min after CpG injection or viral infection. To block cytokines, 500 μg rat IgG (control) or 500 μg anti-IL-10 (JES5-2A5) was injected i.p. into WT mice 1 day and 3 days after C13 infection.

ELISAs

Cytokine and chemokine serum levels were determined by ELISA kits according to the manufacturer's instructions (CCL2, IL-10, and TGF-β1, R&D; CCL7 and CCL12, Bender Med Systems). ATP and AST/ALT serum levels were determined by a luciferin-luciferase assay using an ATP assay kit (Toyo Ink) and a Fuji DRI-CHEM 3500 V analyzer (Fuji Medical Systems), respectively, according to the manufacturer's instructions.

Flow Cytometric Analysis and Cell Sorting

Antibodies against the following molecules were used for flow cytometric analysis and cell sorting: CD3ε (145-2C11), CD11b (M1/70), CD11c (N418), TER119 (TER119), CD19 (MB19-1), CD40 (1C10), CD80 (16-10A1), CD86 (GL19), NK1.1 (PK136), MHC class II (I-A/I-E; M-15/114.15.2), α_V (RMV-7), β_3 (2C9.G3), PD-1 (RMP1-30) (all from eBioscience), F4/80 (BM8) (Biolegend), and Ly6c (AL-219) (BD), Stabilin-2 (#34-2) (MBL), Tryo-3 (109646), Axl (175128) and MerTK (108921) (all from R&D). Antibodies against Tim-1 (RMT1-17), Tim-3 (RMT3-23), and Tim-4 (RMT4-53) were as described previously (Nakayama et al, 2009). To analyze hemophagocytosis, two protocols were used. First, peripheral blood (PB) samples were collected into heparin-containing tubes and immediately maintained on ice. Red blood cells were lysed by adding 10 ml ACK buffer to the samples and keeping them on ice for 10 min. After washing with cold PBS, the samples were stained with APC-anti-CD11c, PE-anti-CD11b, and FITC-anti-TER119. This protocol detected apoptotic erythroid cells exposed on Mo-DC surfaces, including cells attached to Mo-DC PS receptors or undergoing phagocytosis. Second, a recently reported protocol was used to detect the intracellular localization of apoptotic erythroid cells (Zoller et al, 2011). In detail, TER119 exposed on MO-DC surfaces was first blocked with saturating amounts of an unlabeled Ab against TER119 (10 μg/10 μl), then permeabilized with a BD Cytofix/Cytoperm kit (BD) and stained with FITC-anti-TER119 and APC-anti-CD11c Abs. Apoptotic cells were detected using PE-annexin V (BD) according to the manufacturer's instructions. To purify inflammatory monocytes, defined as $CX3CR1^{+}Ly6c^{high}CD11b^{+}CD11c^{-}$ cells, BM $CD3\,\varepsilon^{-}CD19^{-}NK1.1^{-}$ cells were pre-enriched from *Cx₃cr1*$^{GFP/+}$ mice using a PE-Cy5-conjugated antibody mixture (CD3 ε, CD19, NK1.1), Cy5 microbeads, and an AutoMACSpro separation system

(Miltenyi Biotec). The cells were then stained with biotin-anti-Ly6c, PE-anti-CD11b, and APC-anti-CD11c antibodies, secondarily labeled with streptavidin-PE-Cy7, sorted on a MoFlo instrument (Beckman Coulter), and analyzed on a FACSCanto II (BD) in conjunction with FlowJo software (TreeStar).

Intracellular p-ERK and p-p38 staining

PBMCs were obtained from WT mice 4 h after LCMV C13 infection. Red blood cells were lysed, and the PBMCs were fixed with formaldehyde 10 min, permeabilized with ice-cold methanol on ice 20 min, and stained with FITC-anti-TER119, APC-anti-CD11c, and PE-pERK (clone 20A) or p-p38 (clone 30) (all from BD).

CTL Response and Virus Titer Detection

Splenocytes were harvested 9 days after infection. To detect LCMV-specific CTL, splenocytes were stained with FITC-anti-CD8 (KT15) (MBL), APC-anti-CD3ε, and PE-H-2D^{b}-LCMV $gp_{33–41}$ tetramer (MBL). IFN-γ induction was analyzed by stimulating splenocytes with an LCMV H-2D^{b}-binding peptide ($gp_{33–41}$, KAVYNFATM; Peptide Institute), 50 U/ml murine IL-2, and Golgi Stop (BD) prior to incubation with CD8α antibodies. Cells were then fixed and stained with IFN-γ-PE antibodies in PermWash solution (BD) according to the manufacturer's recommendation. For virus titration, MC57G cells were incubated with 10-fold serial dilutions of LCMV-containing serum in a 24-well plate at 37°C for 48 h. Cells were then fixed with 4% formalin, permeabilized with 0.5% Triton X and incubated with 10% fetal bovine serum. After incubation with murine LCMV immunoglobulin G1 (IgG1; Progen Biotechnik) and anti-mouse IgG-horseradish peroxidase (GE Healthcare), the plates were stained using an AEC peroxidase substrate kit (Vector Laboratories), and virus plaques were counted for each well.

Quantitative RT-PCR

Total RNA was extracted using an RNeasy Mini Kit (Qiagen), and cDNA was synthesized using random hexamers and SuperScript III reverse transcriptase. For real-time PCR, cDNA products equivalent to RNA from 2000 cells were amplified using a LightCycler®480 and SYBR Green I Master (Roche Diagnostics). The data were normalized to the levels of *gapdh* RNA expression in each sample. The primers used for real-time PCR were as follows: *Ccr2*, 5’-ATGAGTAACTGTGTGATTGACAAGCA-3’ (sense) and 5’-GCAGCAGTGTGTCATTCCAAGA-3’ (anti-sense); *P2y2*, 5’-CCGAGAGCTCTTTAGCCATTT-3’ (sense) and 5’-GCCATAAGCACGTAACAGACC-3’ (anti-sense); *Gapdh*, 5'-TCCACCACCCTGTTGCTGTA-3' (sense) and 5'-ACCACAGTCCATGCCATCAC-3' (anti-sense); LCMV *GP*, 5'-CATTCACCTGGACTTTGTCAGACTC-3' (sense) and 5'-GCAACTGCTGTGTTCCCGAAAC-3' (anti-sense); LCMV *NP*, 5'-CAATGGACGCAAGCATTGAG-3' (sense) and 5'-GTTCTTCTGCACTGAGCCTCC-3' (anti-sense); *Mfge*8, 5’-GATCTTTCCAAC AACCT GCCTCC-3’ (sense) and 5’-ACCGCTTTCATCCTGGATGAACTC-3’ (ant-sense); *Bai*1, 5'-GCTGGCAGAAGCTGACGAT-3' (sense) and 5'-CACGGAGAT GACCTTAGAGTTG-3' (anti-sense); *Stab*2, 5'-GCTGTCGTCCTGGTTACTG-3' (sense) and 5'-CCAAGGCATCAATGTCATC-3' (antisense); *Tyro*3, 5'-TGCCTGCTTCGGAACTTG-3' (sense) and 5'-GCCTGAGTCGGTACGAATG-3' (antisense); *Axl*, 5'-CCAGTCACAGGACACAGCTC-3' (sense) and 5'-GTGACTCCCTTGGCATTG-3' (anti-sense); *Mertk*, 5'-GGAAAGCGCAGGGACTTAC-3' (sense) and 5'-CTGTGCAGGTGGCATTGTG-3'

(anti-sense); *Gas*6, 5'-GGCATGTGGCAAACT ATCT-3' (sense) and 5'-CGAGCTCACTCTCCTTGAA3' (antisense). Primers were synthesized for *Ccr2*, *P2y2*, LCMV *GP* (Ejrnaes et al, 2006), LCMV *NP* (Djavani et al., 2001), *Mfge8*, *Bai1*, *Stab2*, *Tyro3*, *Axl*, *Mertk*, and *Gas6* by Operon Biotechnology, and for *Gapdh* by Toyobo.

Ex vivo Hemophagocytosis Assay

TER119^{-} Mo-DCs and TER119^{+} erythroid cells or Gr1^{high}Ly6c^{+} granulocytes were separately sorted from the BM of either WT or *Mfge8*$^{-/-}$ mice at 12 h after LCMV C13 infection. The Mo-DCs were precultured in 10 % FCS-RPMI supplemented with 20 ng/ml GM-CSF, washed, then incubated with either isotype Ab cocktails (50 μg/ml of each) or blocking antibodies against Tim1, Tim4, α_v, β_3, or $\alpha_v\beta_5$ (Su et al., 2007) (50 μg/ml of each). TER119^{+} erythroid cells were labeled with pHrodo-SE (0.5 μg/ml, Life Technologies) at room temperature for 30 min, then washed with 10 % FCS PBS after stopping the reaction with 1 ml 100% FCS. To opsonize TER119^{+} erythroid cells, the cells were incubated with goat serum at at 4°C for 1 h, washed, then incubated with anti-goat IgG antibody at 4°C for 1 h. The Mo-DCs (4 x 10^4) and pHrodo-labeled erythroid cells (4 x 10^5), opsonized erythroid cells (4 x 10^5), or granulocytes (2 x 10^5) were co-cultured in 100 μl of 10 % FCS-RPMI supplemented with 20 ng/ml GM-CSF in 96 well U-bottom Ultra-Low Attached plate (Corning) at 37°C for 2 h for Diff-Quick staining and flow cytometry or 24 h for ELISA. To block internalization of apoptotic erythroid cells into Mo-DCs, control DMSO (0.01%) or cytochalasin D (5μM) was added in culture for 2 h, washed out, then 24 h supernatants were subjected to IL-10 ELISA.

Ex vivo Induction of PS and PS receptors by IFN-α

Erythroid cells and granulocytes, sorted from the BM of WT mice, and T cells, B cells, NK cells, sorted from the spleen of WT mice, were stimulated *ex vivo* with different doses of IFN-α for 18 h, then subjected to annexin V staining. In addition, inflammatory monocytes, sorted from the BM of WT mice, were stimulated *ex vivo* with IFN-α (1 x 10^4 U/ml) for 24 h, then, subjected to the analysis of PS receptor expression.

Liver Histology

Livers were isolated 9 days after C13 infection, then fixed in 4% paraformaldehyde, embedded in paraffin, sectioned at 5-μm thickness, and stained with hematoxylin/eosin.

Statistical Analysis

We evaluated the statistical significance of the obtained values by Student's *t*-test. We considered a *P* value <0.05 as significant.

ACKNOWLEDGMENTS

We thank H. Kamioka for secretarial support, Nobuhiko Kamada (Keio University) for the B6.*Ccl2*$^{-/-}$ mice, Shigekazu Nagata (Kyoto University) for the B6.*Mfge8*$^{-/-}$ mice, Dean Sheppard (University of California, San Francisco) for the Ab against integrin $\alpha_v\beta_5$, and Toshitaka Akatsuka (Saitama Medical University) for the LCMV Clone 13. This work was supported by the Takeda Science Foundation (T.O.), the Joint Usage/Research Program of the Medical Research Institute, Tokyo Medical and Dental University (K.S.), a Grant-in-Aid for Scientific Research on Priority Areas from the Ministry of Education, Science, Sports and Culture of Japan (T.O.), Challenging Exploratory Research (T.O.), and Japan Science and Technology Agency, Core Research for Evolutional Science and Technology (CREST) (T.O.). H.O. and N.O. conceived the

study, performed experiments, analyzed data, and wrote the manuscript. T.S., S.Y., K.K., and M.H. assisted N.O. with experiments. H.A., H.Y., K.A., K.H., N.T., M.H., and K.S. provided reagents, mice, discussion, and advice on some parts of this study. T.O. supervised the overall project and wrote the manuscript. The authors declare no competing financial interests.

REFERENCES

Akakura, S., Singh, S., Spataro, M., Akakura, R., Kim, Jong-Il., Albert, M.L., and Birge, R.B. (2003). The opsonin MFG-E8 is a ligand for the αvβ5 integrin and triggers DOCK180-dependent Rac1 activation for the phagocytosis of apoptotic cells. Exp. Cell. Res. *292*, 403-416.

Atarashi, K., Tanoue, T., Shima, T., Imaoka, A., Kuwahara T., Momose, Y., Cheng, G., Yamasaki, S., Saito, T., Ohba, Y., et al. (2011). Induction of colonic regulatory T cells by indigenous Clostridium species. Science *331*, 337-341.

Auffray, C., Sieweke, M.H., and Geissmann, F. (2009). Blood monocytes: development, heterogeneity, and relationship with dendritic cells. Annu. Rev. Immunol. *27*, 669-692.

Banchereau, J. J., Briere, F., Caux, C., Davoust, J., Lebecque, S., Liu, Y.J., Pulendran, B., Palucka, K. (2000). Immunobiology of dendritic cells. Annu. Rev. Immunol. *18*, 767-811.

Barber, D.L., Wherry, E.J., Masopust, D., Zhu, B., Allison, J.P., Sharpe, A.H., Freeman, G.J., and Ahmed, R. (2006). Restoring function in exhausted CD8 T cells during chronic viral infection. Nature *439*, 682-687.

Behrens, E.M., Canna, S.W., Slade, K., Rao, S., Kreiger, P.A., Paessler, M., Kambayashim, T., Koretzky, G,A. (2011). Repeated TLR9 stimulation results in macrophage activation syndrome-like disease in mice. J. Clin. Invest. *121*, 2246-2277.

Boring, L., Gosling, J., Chensue, S.W., Kunkel, S.L., Farese, R.V. Jr., Broxmeyer, H.E., and Charo, I.F. (1997). Impaired monocyte migration and reduced type 1 (Th1) cytokine responses in C-C chemokine receptor 2 knockout mice. J. Clin. Invest. *100*, 2552-2561.

Brooks, D.G., Trifilo, M.J., Edelmann, K.H., Teyton, L., McGavern, D.B., and Oldstone, M.B. (2006). Interleukin-10 determines viral clearance or persistence in vivo. Nat. Med. *12*, 1301-1309.

Budiani, D.R., Hutahaean, S., Haryana, S.M., Soesatyo, M.H. and Sosroseno, W. (2002). Interleukin-10 levels in Epstein-Barr virus-associated nasopharyngeal carcinoma. J. Microbiol. Immunol. Infect. *35*, 265-268.

Byrne, A., and Reen, D.J. (2002). Lipopolysaccharide induces rapid production of IL-10 by monocytes in the presence of apoptotic neutrophils. J. Immunol. *168*, 1968-1977.

Clark, I.A. (2007). How TNF was recognized as a key mechanism of disease. Cytokine Growth Factor Rev*. 18,* 335-343.

Clerici, M., Balotta, C., Salvaggio, A., Riva, C., Trabattoni, D., Papagno, L., Berlusconi, A., Rusconi, S., Villa, M.L., Moroni, M., et al. (1996). Human immunodeficiency virus (HIV) phenotype and interleukin-2/interleukin-10 ratio are associated markers of protection and progression in HIV infection. Blood *88*, 574-579.

Cooper, M.D. and Alder, M.N. (2006). The evolution of adaptive immune systems. Cell *124*, 815-822.

Djavani, M., Rodas, J., Lukashevich, I.S., Horejsh, D., Pandolfi, P.P., Borden, K.L., and Salvato, M.S. (2001). Role of the promyelocytic leukemia protein PML in the interferon sensitivity of lymphocytic choriomeningitis virus. *J. Virol*. *75*, 6204-6208.

Domínguez, P.M, and Ardavín, C. (2010). Differentiation and function of mouse monocyte-derived dendritic cells in steady state and inflammation. Immunol. Rev. *234*, 90-104.

Ejrnaes, M., Filippi, C.M., Martinic, M.M., Ling, E.M., Togher, L.M., Crotty, S., and von Herrath, M.G. Resolution of a chronic viral infection after interleukin-10 receptor blockade. *J. Exp. Med*. 203, 2461-2472 (2006).

Elliott, M.R., Chekeni, F.B., Trampont, P.C., Lazarowski, E.R., Kadl, A., Walk, S.F., Park, D., Woodson, R.I., Ostankovich, M, Sharma, P., et al. (2009). Nucleotides released by apoptotic cells act as a find-me signal to promote phagocytic clearance. Nature *461*, 282-286.

Geissmann, F., Manz, M.G., Jung, S., Sieweke, M.H., Merad, M., and Ley, K. (2010). Development of monocytes, macrophages, and dendritic cells. Science *327*, 656-661.

Hanayama, R., Tanaka, M., Miwa, K., Shinohara, A., Iwamatsu, A., and Nagata, S. (2002). Identification of a factor that links apoptotic cells to phagocytes. Nature *417*, 182-187.

Hanayama, R., Tanaka, M., Miyasaka, K., Aozasa, K., Koike, M., Uchiyama, Y., and Nagata, S. (2004). Autoimmune disease and impaired uptake of apoptotic cells in MFG-E8-deficient mice. Science *304*, 1147-1150.

Janka, G.E. (2007). Hemophagocytic syndrome. Blood Rev. *21*, 245-253.

Jung, S., Aliberti, J., Graemmel, P., Sunshine, M.J., Kreutzberg, G.W., Sher, A., and Littman, D.R. (2000). Analysis of fractalkine receptor CX_3CR1 function by targeted deletion and green fluorescent protein reporter gene insertion. Mol. Cell. Biol. *20*, 4106-4114.

Kawai, T., and Akira, S. (2010). The role of pattern-recognition receptors in innate immunity: update on Toll-like receptors. Nat. Immunol. *11*, 373-384.

Kawane, K., Fukuyama, H., Kondoh, G., Takeda, J., Ohsawa, Y., Uchiyama, Y., and Nagata, S. (2001). Requirement of DNase II for definitive erythropoiesis in the mouse fetal liver. Science *292*, 1546-1549.

Kim, S., Elkon, K.B., and Ma, X. (2004). Transcriptional suppression of interleukin-12 gene expression following phagocytosis of apoptotic cells. Immunity *21*, 643-653.

Kobasa, D., Jones, S.M., Shinya, K., Kash, J.C., Copps, J., Ebihara, H., Hatta, Y., Kim, J.H., Halfmann, P., Hatta, M., et al. (2007). Aberrant innate immune response in lethal infection of macaques with the 1918 influenza virus. Nature *445*, 319-323.

Kobayashi, N., Karisola, P., Pena-Cruz, V., Dorfman, D.M., Jinushi, M., Umetsu, S.E., Butte, M.J., Nagumo, H., Chernova, I., Zhu, B., et al. (2007). TIM-1 and TIM-4 glycoproteins bind phosphatidylserine and mediate uptake of apoptotic cells. Immunity *27*, 927-940.

Lambeth, J.D. (2007). Nox enzymes, ROS, and chronic disease: an example of antagonistic pleiotropy. Free Radic. Biol. Med. *43*, 332-347.

Larroche, C., and Mouthon, L. (2003). Pathogenesis of hemophagocytic syndrome (HPS). Autoimmun. Rev. *3*, 69-75.

Leon, B., Lopez-Bravo, M., and Ardavin, C. (2007). Monocyte-derived dendritic cells formed at the infection site control the induction of protective T helper 1 responses against Leishmania. Immunity *26*, 519-531.

Lu, B., Rutledge, B.J., Gu, L., Fiorillo, J., Lukacs, N.W., Kunkel, S.L., North R., Gerard, C., and Rollins, B.J. (1998). Abnormalities in monocyte recruitment and cytokine expression in monocyte chemoattractant protein 1-deficient mice. J. Exp. Med. *187*, 601-608.

Maakaroun, N.R., Moanna, A., Jacob, J.T., and Albrecht, H. (2010). Viral infections associated with haemophagocytic syndrome. Rev. Med. Virol. *20*, 93-105.

Martin, S.J., Finucane, D.M., Amarante-Mendes, G.P., O'Brien, G.A., and Green, D.R. (1996). Phosphatidylserine externalization during CD95-induced apoptosis of cells and cytoplasts requires ICE/CED-3 protease activity. J. Biol. Chem. *271*, 28753-28756.

Matloubian, M., Somasundaram, T., Kolhekar, S.R., Selvakumar, R., and Ahmed, R. (1990). Genetic basis of viral persistence: single amino acid change in the viral glycoprotein affects ability of lymphocytic choriomeningitis virus to persist in adult mice. J. Exp. Med. *172*, 1043-1048.

Medzhitov, R. and Janeway, C.A., Jr. (1997). Innate immunity: the virtues of a nonclonal system of recognition. Cell *91*, 295-298.

Miyanishi, M., Tada, K., Koike, M., Uchiyama, Y., Kitamura, T, and Nagata, S. (2007). Identification of Tim4 as a phosphatidylserine receptor. Nature *450*, 435-439.

Nagata, S., Hanayama, R., and Kawane, K. (2010). Autoimmunity and the clearance of dead cells. Cell *140*, 619-630.

Nakayama, M., Akiba, H., Takeda, K., Kojima, Y., Hashiguchi, M., Azuma, M., Yagita, H., and Okumura, K. (2009). Tim-3 mediates phagocytosis of apoptotic cells and cross-presentation. Blood *113*, 3821-3830.

Nordoy, I. Müller, F., Nordal, K.P., Rollag, H., Lien, E., Aukrust, P., and Froland, S.S. (2000). The role of the tumor necrosis factor system and interleukin-10 during cytomegalovirus infection in renal transplant recipients. J. Infect. Dis. *181*, 51-57.

Randolph GJ, Inaba K, Robbiani DF, Steinman RM, and Muller WA. (1999). Dofferentiation of phagocytic monocytes into lymph node dendritic cells in vivo. Immunity *11*, 753-761.

Rodriguez-Manzanet, R., Meyers, J.H., Balasubramanian, S., Slavik, J., Kassam, N., Dardalhon, V., Greenfield, E.A., Anderson, A.C., Sobel, R.A., Hafler, D.A., et al. (2008). TIM-4 expressed on APCs induces T cell expansion and survival. J. Immunol. *180*, 4706-4713.

Roers, A., Siewe, L., Strittmatter, E., Deckert, M., Schlüter, D., Stenzel, W., Gruber, A.D., Krieg, T., Rajewsky, K., and Müller, W. (2004). T cell-specific inactivation of the interleukin 10 gene in mice results in enhanced T cell responses but normal innate responses to lipopolysaccharide or skin irradiation. J. Exp. Med. *200*, 1289-1297.

Rouse, B.T., and Sehrawat, S. (2010). Immunity and immunopathology to viruses: what decides the outcome? Nat. Rev. Immunol. *10*, 514-526.

Schaer, C.A., Schoedon, G., Imhof, A., Kurrer, M.O., and Schaer, D.J. (2006). Constitutive endocytosis of CD163 mediates hemoglobin-heme uptake and determines the noninflammatory and protective transcriptional response of macrophages to hemoglobin. Circ. Res. *99*, 943-950.

Schaer, D.J., Schaer, C.A., Schoedon, G., Imhof, A., and Kurrer, M.O. (2006). Hemophagocytic macrophages constitute a major component of heme oxygenase expression in sepsis. Eur. J. Hematol. *77*, 432-436.

Schneider, D.S., and Ayres, J.S. (2008). Two ways to survive infection: what resistance and tolerance can teach us about treating infectious diseases. Nat. Rev. Immunol. *8*, 889-895.

Serbina, N.V., Jia T., Hohl, T.M., and Pamer, E.G. (2008). Monocyte-mediated defense against microbial pathogens. Annu. Rev. Immunol. *26*, 421-452.

Serbina, N.V., and Pamer, G. (2006). Monocyte emigration from bone marrow during bacterial infection requires signals mediated by chemokine receptor CCR2. Nat. Immunol. *7*, 311-317.

Sevilla, N. Kunz, S., Holz, A., Lewicki, H., Homann, D., Yamada, H., Campbell, K.P., de La Torre, J.C., and Oldstone, M.B. (2000). Immunosuppression and resultant viral persistence by specific viral targeting of dendritic cells. J. Exp. Med. *192*, 1249-1260.

Stranges, P.B., Watson, J., Cooper, C.J., Choisy-Rossi, C.M., Stonebraker, A.C, Beighton, R.A., Hartig, H., Sundberg, J.P., Servick, S., Kaufmann, G., et al. (2007). Elimination of antigen-presenting cells and autoreactive T cells by Fas contributes to prevention of autoimmunity. Immunity *26*, 629-641.

Su G, Hodnett M, Wu N, Atakilit A, Kosinski C, Godzich M, Huang XZ, Kim JK, Frank JA, Matthay MA, et al. (2007). Integrin $\alpha_v\beta_5$ regulates lung vascular permeability and pulmonary endothelial barrier function. Am. J. Respir. Cell Mol. Biol. *36*, 377-386.

Takahashi, K., Nakamura, T., Koyanagi, M., Kato, K., Hashimoto, Y., Yagita, H., and Okumura, K. (1990). A murine very late activation antigen-like extracellular matrix receptor involved in CD2- and lymphocyte function-associated antigen-1- independent killer-target cell interaction. J. Immunol. *145*, 4371-4379.

Tarumi, T., Sawada, K., Sato, N., Kobayashi, S., Takano, H., Yasukouchi, T., Takashashi, T., Sekiguchi, S., and Koike, T. (1995). Interferon-α-induced apoptosis in human erythroid progenitors. Exp. Hematol. *23*, 1310-1318.

Voll, R.E., Herrmann, M., Roth, E.A., Stach, C., Kalden, J.R., and Girkontaite, I. (1997). Immunosuppressive effects of apoptotic cells. Nature *390*, 350-351.

Waibler, Z., Anzaghe, M., Konur, A., Akira, S., Müller, W., and Kalinke, U. (2008). Excessive CpG 1668 stimulation triggers IL-10 production by cDC that inhibits IFN-α responses by pDC. Eur. J. Immunol. *38*, 3127-3137.

Xiao, S. Najafian, N., Reddy, J., Albin, M., Zhu, C., Jensen, E., Imitola, J., Korn, T., Anderson, A.C., Zhang, Z., et al. (2007) Differential engagement of Tim-1 during activation can positively or negatively costimulate T cell expansion and effector function. J. Exp. Med. *204*, 1691-1702.

Xiao, S. Zhu B, Jin H, Zhu C, Umetsu DT, DeKruyff RH, and Kuchroo VK. (2011). Tim-1 stimulation of dendritic cells regulates the balance between effector and regulatory T cells. *Eur. J. Immunol. 41,* 1539-1549.

Yasuda, M., Hasunuma, Y., Adachi, H., Sekine, C., Sakanishi, T., Hashimoto, H., Ra, C., Yagita, H., and Okumura, K. (1995). Expression and function of fibronectin binding integrins on rat mast cells. Int. Immunol, *7*, 251-258.

Yoshida, H., Okabe, Y., Kawane, K., Fukuyama, H., and Nagata, S. (2005). Lethal anemia caused by interferon-β produced in mouse embryos carrying undigested DNA. Nat. Immunol. 6, 49-56.

Zinkernagel, R.M., Haenseler, E., Leist, T., Cerny, A., Hengartner, H., and Althage, A. (1986). T cell-mediated hepatitis in mice infected with lymphocytic choriomeningitis virus. Liver cell destruction by H-2 class I-restricted virus-specific cytotoxic T cells as a physiological correlate of the ^{51}Cr-release assay? J. Exp. Med. *164*, 1075-1092.

Zoller, E.E., Lykens, J.E., Terrell, C.E., Aliberti, J., Filipovich, A.H., Henson, P.M., and Jordan, M.B. (2011). Hemophagocytosis causes a consumptive anemia of inflammation. J. Exp. Med. *208*, 1203-1214.

Figure legends

Figure 1. TLR Ligands Induce Hemophagocytosis

(A) Hemophagocytosis (%) 18 h after an injection of PBS (vehicle) or the indicated TLR or NLR ligand. (B) Sorted $CD11c^{+}TER119^{+}$ cells from the BM of CpG-injected mice were stained with Diff-Quick. Red and black arrows indicate hemophagocytosed and attached erythroid cells, respectively. Original magnification, x100. (C) Sorted $CD11c^{+}TER119^{+}$ cells from the PB of CpG injected mice were analyzed by electron microscope. Scale bar, 1 μm. Arrows indicate hemophagocytosed erythroid cells. (D) Cell-surface staining of $CD11c^{+}TER119^{+}$ cells in the peripheral blood (PB) of 200-mg CpG-injected WT mice after blocking with an unlabeled anti-TER119 Ab. (E, F) Representative flow cytometry (FCM) results (E) and percentage (F) of intracellular $CD11c^{+}TER119^{+}$ cells in the PB of WT mice 18 h after injection of the indicated doses of CpG. Data represent the mean ± s.d. of three independent experiments. $*P < 0.01$ and $**P < 0.05$.

Figure 2. CCR2 Is Involved in Developing CpG-Induced Hemophagocytosis

(A-C) Kinetics of serum CCL2 (A), CCL7 (B), and CCL12 (C) production in WT mice after 200-μg CpG injection. (D) Relative *Ccr2* mRNA expression in the indicated cell populations from WT mice 18 h after 200-μg CpG injection. BMDC, bone marrow-derived DCs. (E, F) Percentage of $CD11c^{+}TER119^{+}$ cells in the PB (E) and BM (F) of the indicated mice 18 h after 200-μg CpG injection. Data represent the mean ± s.d. of three independent experiments. $*P < 0.01$, $**P < 0.05$.

Figure 3. "Find Me" and "Eat Me" Signals in CpG-Induced Hemophagocytosis

(A) Serum ATP level over time in WT mice after 200-μg CpG injection. (B) Relative *P2y2* mRNA expression in $CD11c^+TER119^+$ cells from the PB and the indicated BM-derived cell populations 18 h after 200-μg CpG injection. (C) Percentage of $CD11c^+TER119^+$ cells in the PB of WT mice 18 h after 200-μg CpG injection with 6 mg suramin. (D) Percentage of annexin V^+ cells among $TER119^+$ cells in the PB of WT mice over time after PBS (vehicle) or 200-μg CpG injection. (E) Expression of "eat me" signal receptors on CpG-induced $CD11c^+TER119^+$ cells. Shaded histograms represent cells stained with mAbs for the indicated molecules, and open histograms show labeling with isotype controls. (F) Impaired CpG-induced hemophagocytosis in WT mice treated with blocking antibodies against Tim1, Tim4, α_v, and β_3. The proportion of $CD11c^+TER119^+$ cells 18 h after 200-μg CpG injection with isotype control Ab cocktails (500 μg each) or the indicated antibody mixtures (500 μg each). Ab mix: mixture of antibodies against Tim1, Tim4, α_v, and β_3. (G) IL-10 serum levels 24 hr after the indicated treatments. Data represent the mean ± s.d. of three independent experiments. $*P < 0.01$.

Figure 4. Essential Role of Type I IFNs in C13-Induced Hemophagocytosis

(A, B) Kinetics of serum IFN-α (A) and IFN-β (B) production in WT mice after 2×10^6 pfu C13 infection. (C) Representative flow cytometry (FCM) profiles of $CD11c^+TER119^+$ cells in the PB of WT and *Ifnar*$1^{-/-}$ mice 24 h after 2×10^6 pfu C13 infection. (D, E) The percentage of $CD11c^+TER119^+$ cells (D) and annexin V^+ cells among $TER119^+$ cells (E) in the PB of WT mice 4 h and 24 h after injection of 2×10^6 pfu C13, respectively. (F, G) Expression of "eat me" signal receptors on

$CD11c^{+}TER119^{+}$ cells in the PB of WT (F) and *Ifnar1*$^{-/-}$ (G) mice 24 h after 2 x 10^6 pfu C13 infection. Shaded histograms represent cells stained with mAbs specific for the indicated molecules, and open histograms show labeling with isotype controls.

Figure 5. Hemophagocytosis-Dependent IL-10 Production from MO-DCs upon C13 Infection

(A) C13-induced hemophagocytosis in WT mice treated with either isotype control Ab cocktails (500 μg each) or blocking antibodies against PS receptors (500 μg each). (B) IL-10 and TGF-β1 serum levels 24 h after C13 infection with the injection of isotype control Ab cocktails (500 μg each), Abs to block PS receptors or neutralize IL-10. (C) A representative FCM profile of IL-10 Venus expression in the indicated cell populations from the PB of *Il10*^{Venus} reporter mice 24 h after C13 infection. (D) The absolute number of cells expressing IL-10 Venus in the indicated cell populations from the PB of *Il10*^{Venus} reporter and WT mice 1 and 9 days after C13 infection. Data represent the mean ± s.d. from three independent experiments. *$P < 0.01$.

Figure 6. Critical role of MFG-E8-integrin signal in IL-10 production from Mo-DCs

(A-F) *Ex vivo* hemophagocytosis assay. $TER119^{-}$ Mo-DCs and $TER119^{+}$ erythroid cells were separately sorted from the BM of LCMV C13 infected WT or *Mfge8*$^{-/-}$ mice. The Mo-DCs were pretreated with control rat Ig (A, left panel, and C) or Abs to block PS receptors (B, right panel, and D), and co-cultured with pHrodo-labeled $TER119^{+}$ erythroid cells for 2 h. The cells were stained with Diff-Quick. Red arrows indicate hemophagocytes. Original magnification, x20 (A). Representative FCM profiles of Mo-DCs co-cultured with unlabeled- (B), pHrodo-labeled-erythroid cells (C, D). IL-10

level in the indicated co-culture supernatants (E, F). Data represent the mean ± s.d. of three independent experiments. *$P < 0.01$.

Figure 7. Physiological Significance of C13 Infection-Induced Hemophagocytosis

(A-F) Hemophagocytosis (%) (A) and IL-10 serum levels (B) 24 h after C13 infection. The percentage of LCMV GP_{33-41}-specific $CD8^+$ T cells in the spleen (C), titer of LCMV C13 in the serum (D), and level of AST/ALT in the serum (E) of WT and *Cd11c*-Cre *Il10*$^{fl/fl}$ (CKO) mice 9 days after C13 infection, and survival (%) of WT or CKO mice after LCMV C13 infection (F). Data represent the mean ± s.d. of three independent experiments. *$P < 0.01$.

Figure 1. Ohyagi, et al.

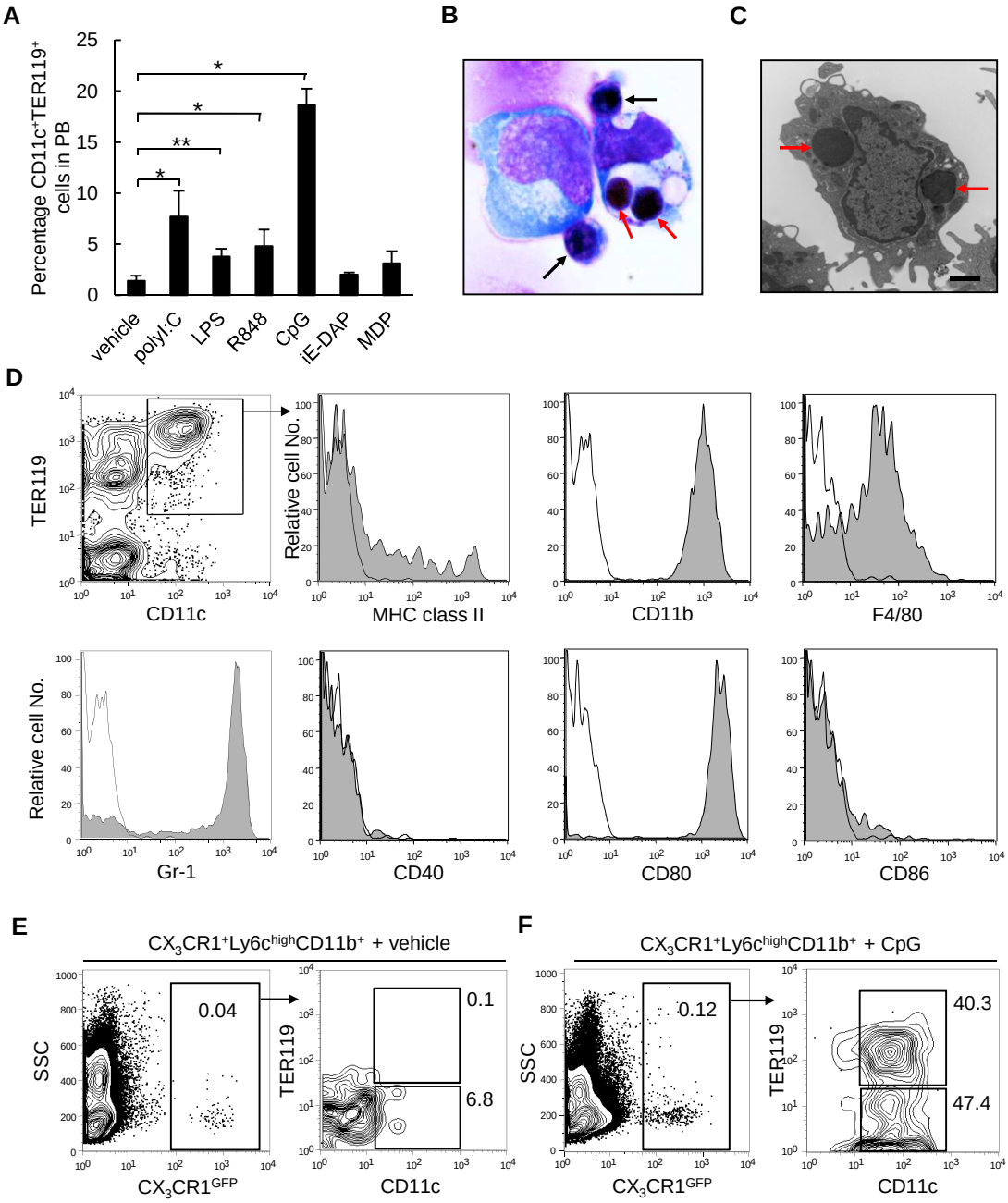

Figure 2. Ohyagi, et al.

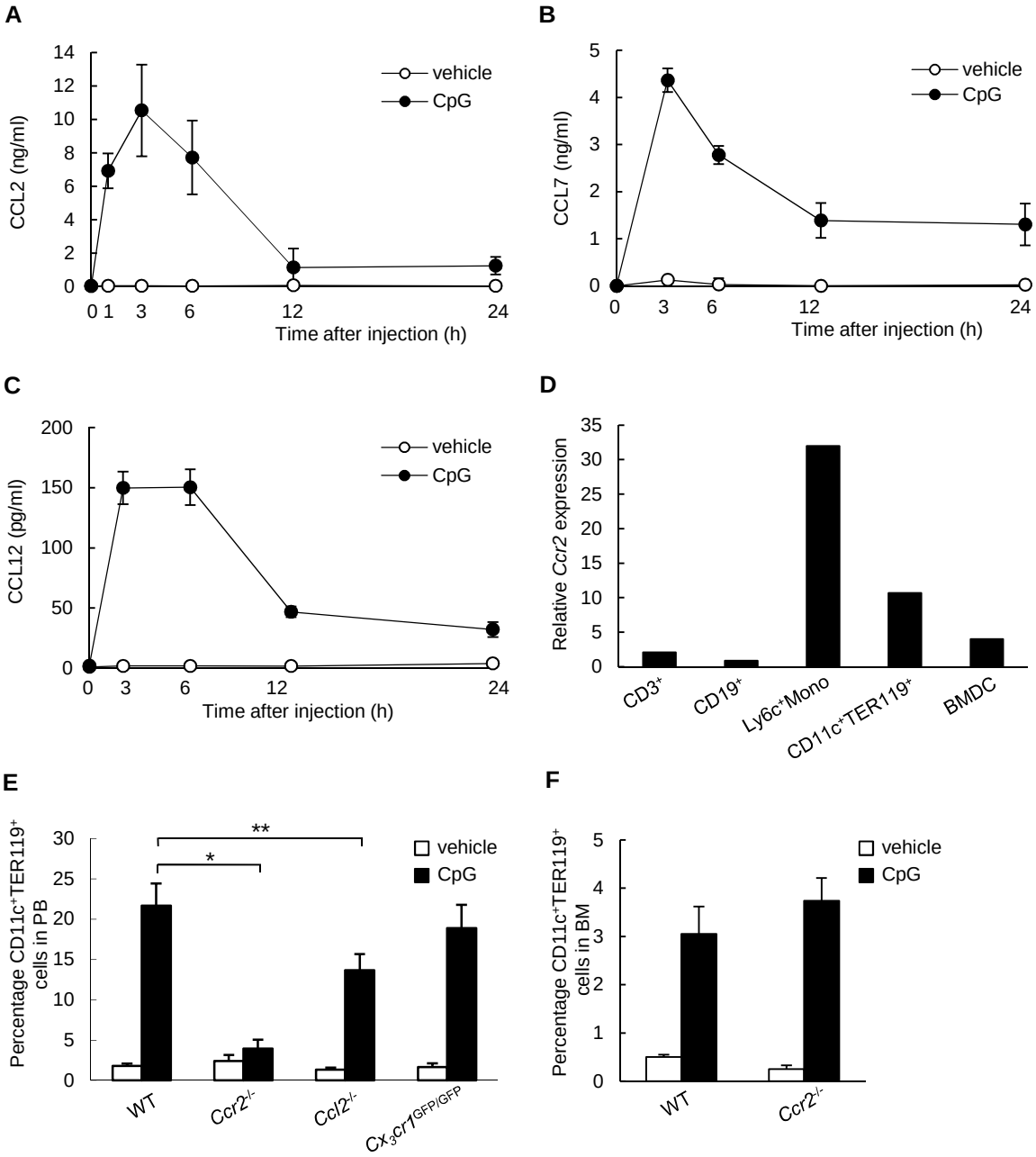

Figure 3. Ohyagi, et al.

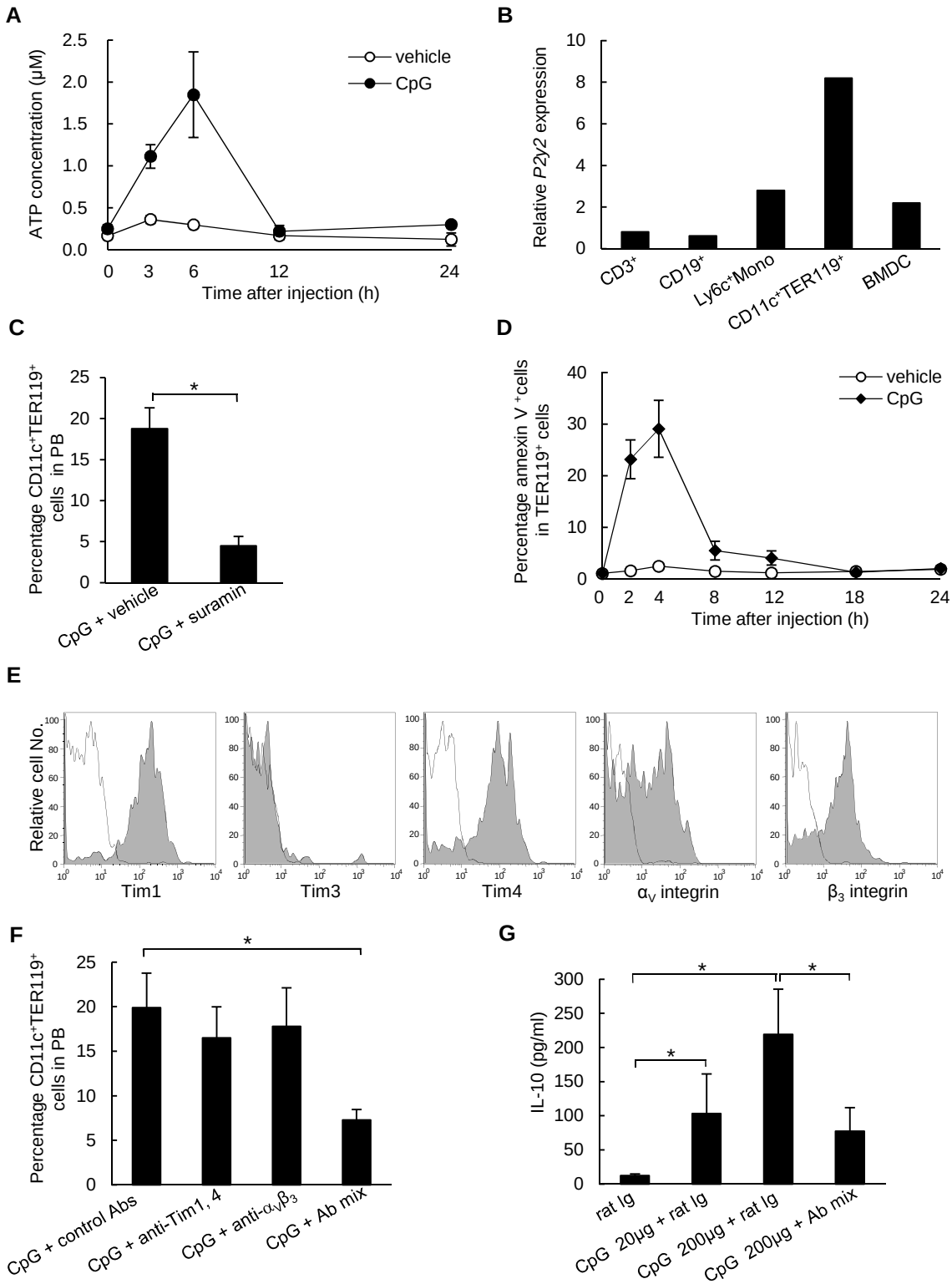

Figure 4. Ohyagi, et al.

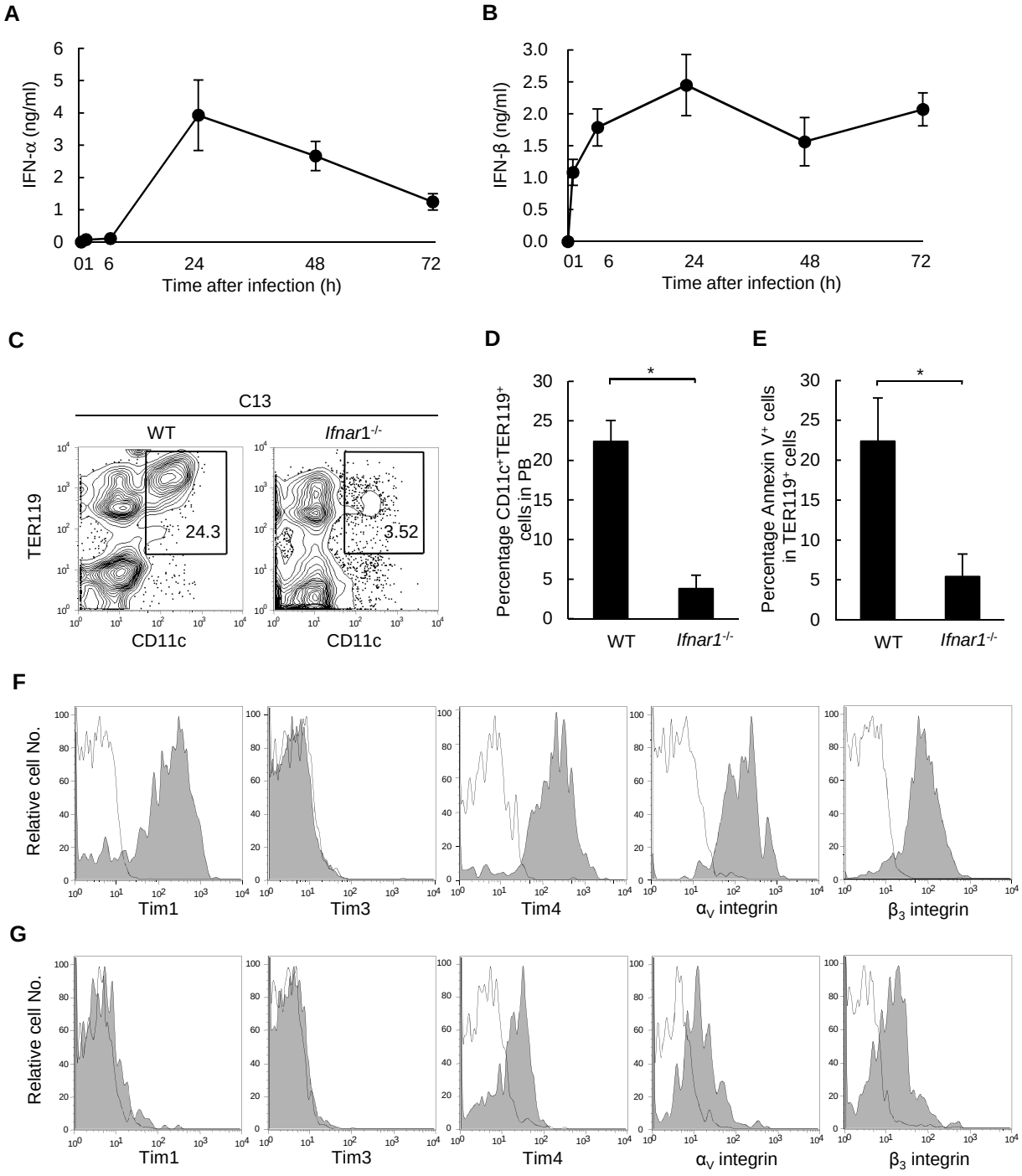

Figure 5. Ohyagi, et al.

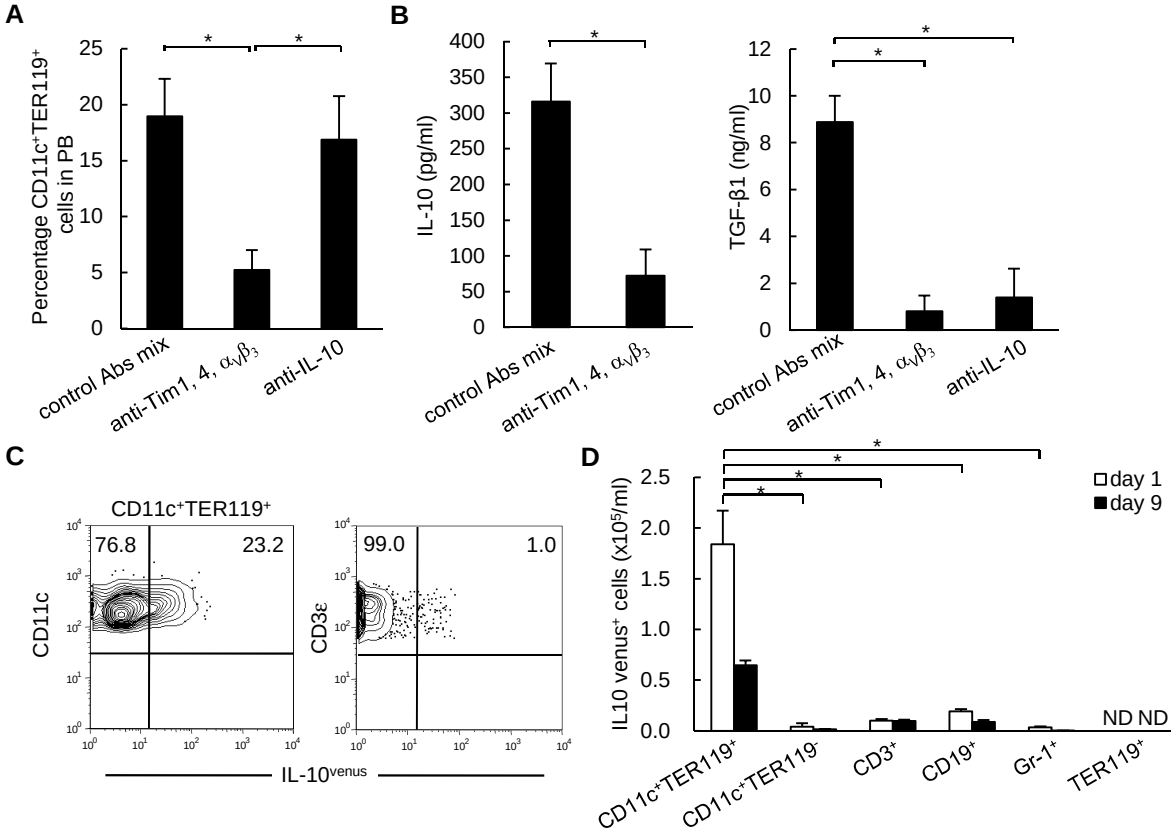

Figure 6. Ohyagi, et al.

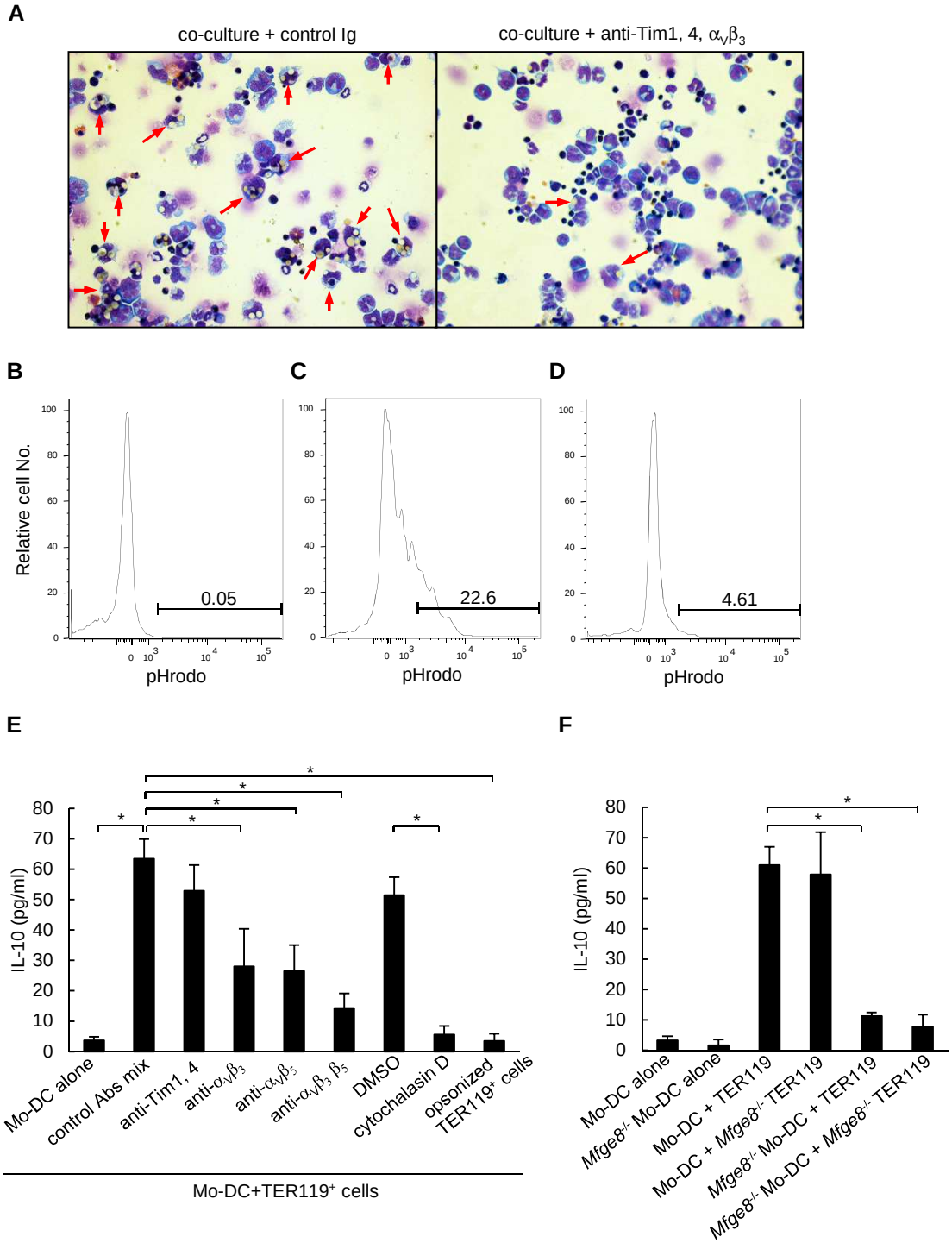

Figure 7. Ohyagi, et al.

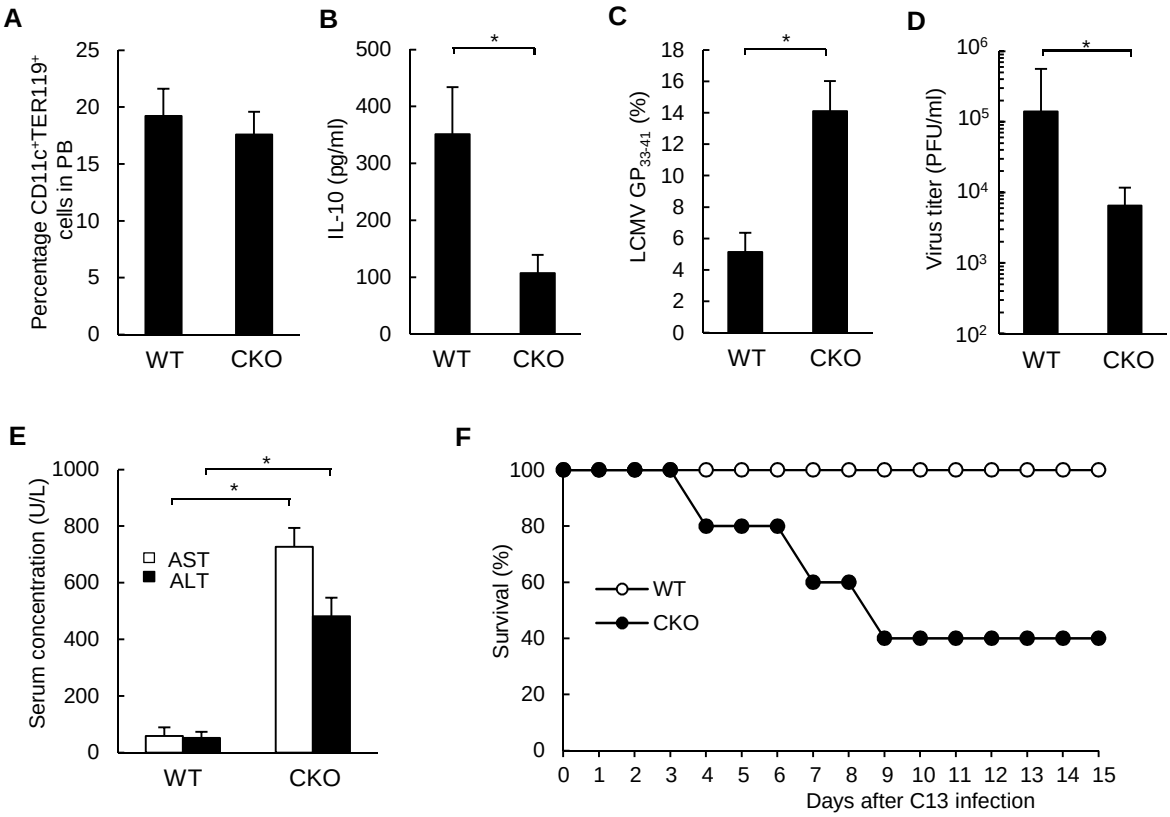

Supplementary Information

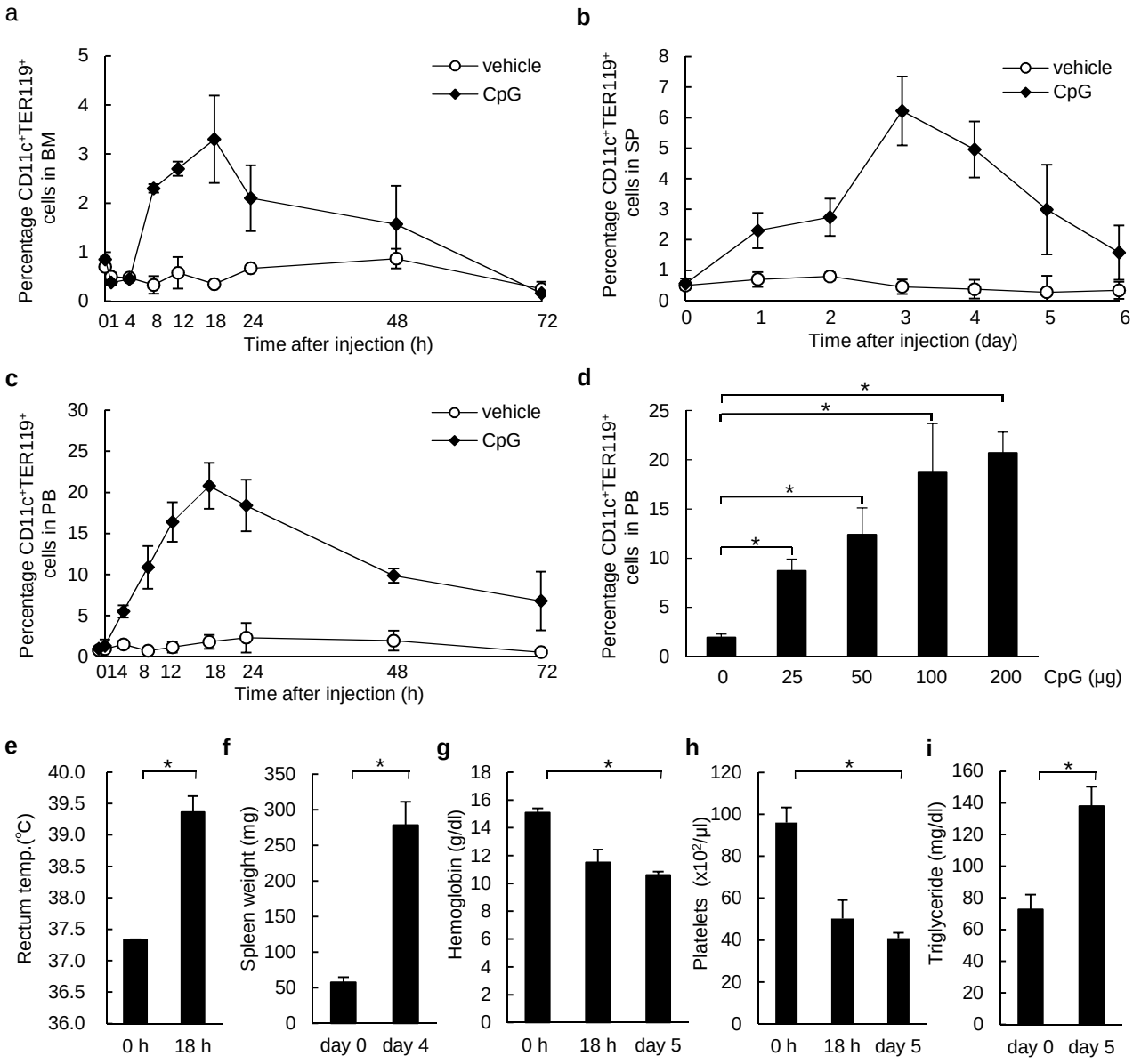

Figure S1. Hemophagocytosis in CpG-injected mice. (**a**-**c**) Time course of the percentage of CD11c$^+$TER119$^+$ cells in the bone marrow (BM) (**a**), spleen (SP) (**b**), and PB (**c**) of WT mice after vehicle (PBS) or 200-μg CpG injection. (**d**) Percentage of CD11c$^+$TER119$^+$ cells in the PB of WT mice 18 h after injection of the indicated doses of CpG. (**e**-**i**) Clinical parameters for HPS, i.e., rectal temperature (^{o}C) (**e**), spleen weight (mg) (**f**), hemoglobin (g/dl) (**g**), platelets (x10^2/μl) (**h**), and triglycerides (mg/dl) (**i**) were evaluated at 18 h (**e**) and at the indicated time points (**e**-**i**), after an injection of PBS (vehicle) or 200-μg CpG. Data represent the mean ± s.d. of three independent experiments. *P < 0.01.

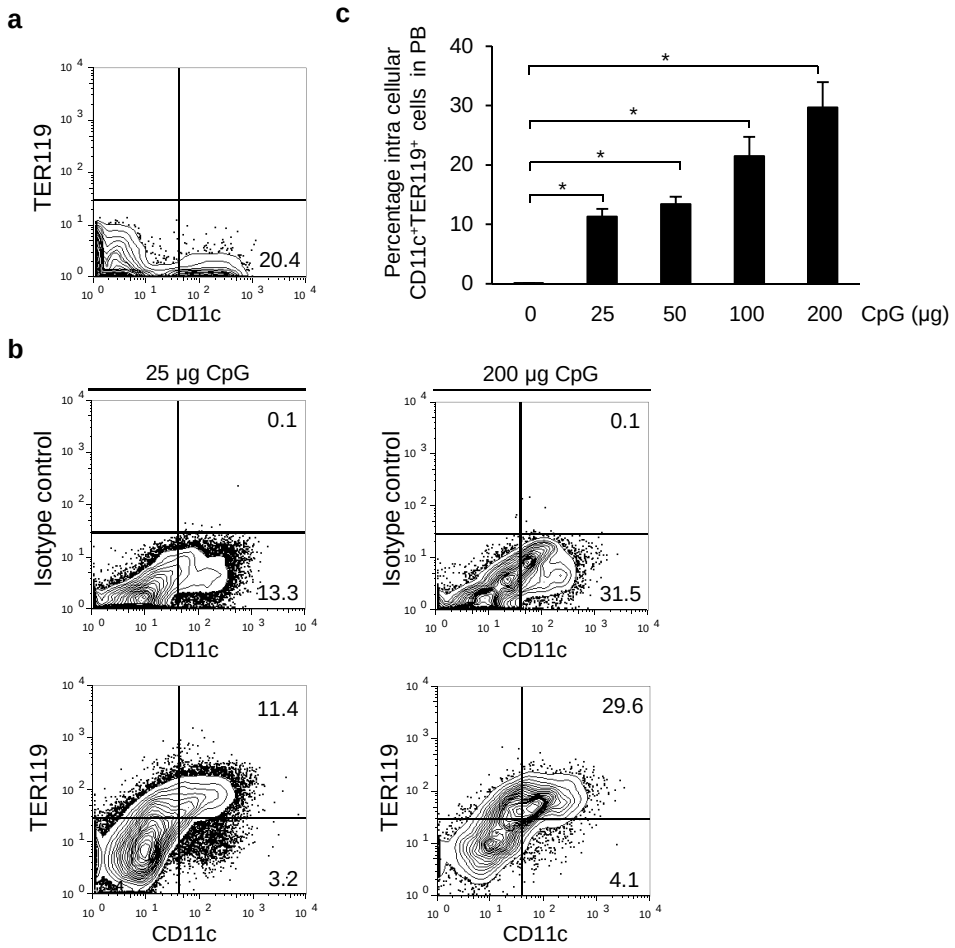

Figure S2. Intracellular detection of TER119$^+$ cells inside CD11c$^+$ cells. (**a**) Cell-surface staining of CD11c$^+$TER119$^+$ cells in the peripheral blood (PB) of 200-μg CpG-injected WT mice after blocking with an unlabeled anti-TER119 Ab. (**b**, **c**) Representative flow cytometry (FCM) results (**b**) and percentage (**c**) of intracellular CD11c$^+$TER119$^+$ cells in the PB of WT mice 18 h after injection of the indicated doses of CpG. Data represent the mean ± s.d. of three independent experiments. *P < 0.01.

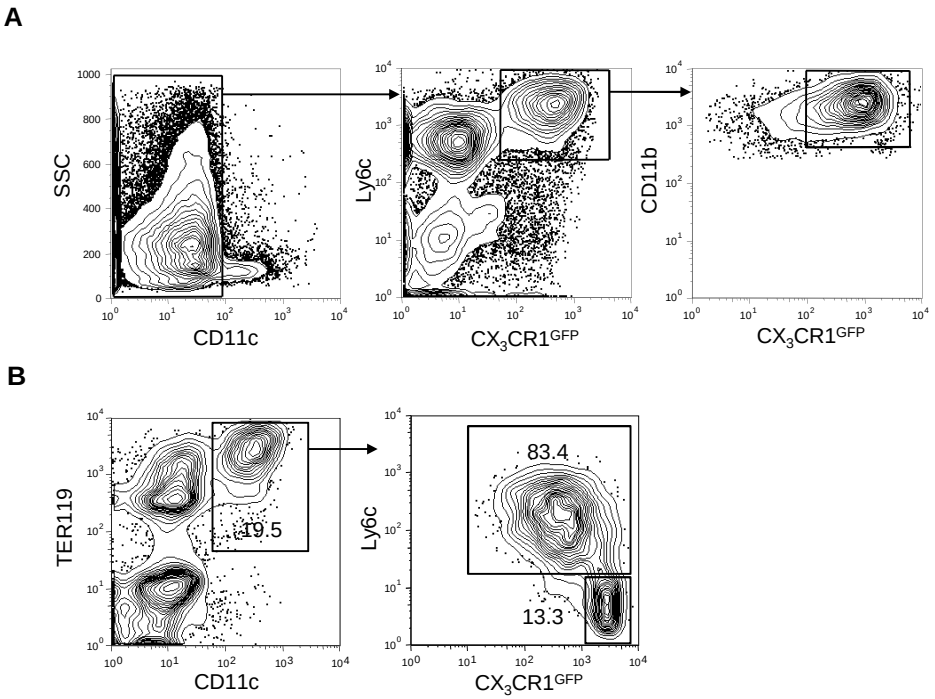

Figure S3. Inflammatory monocyte-derived DCs are the major hemophagocytes in CpG-injected mice. (**A**) Purification of inflammatory monocytes, defined as Ly6c^{+}CX$_3$CR1$^{GFP/+}$CD11b^{+}CD11c^{-} cells, from the BM of *Cx$_3$cr1*$^{GFP/+}$ mice. (**B**) Representative FCM profiles of CD11c^{+} TER119^{+} cells in the PB of *Cx$_3$cr1*$^{GFP/+}$ mice 18 h after CpG injection.

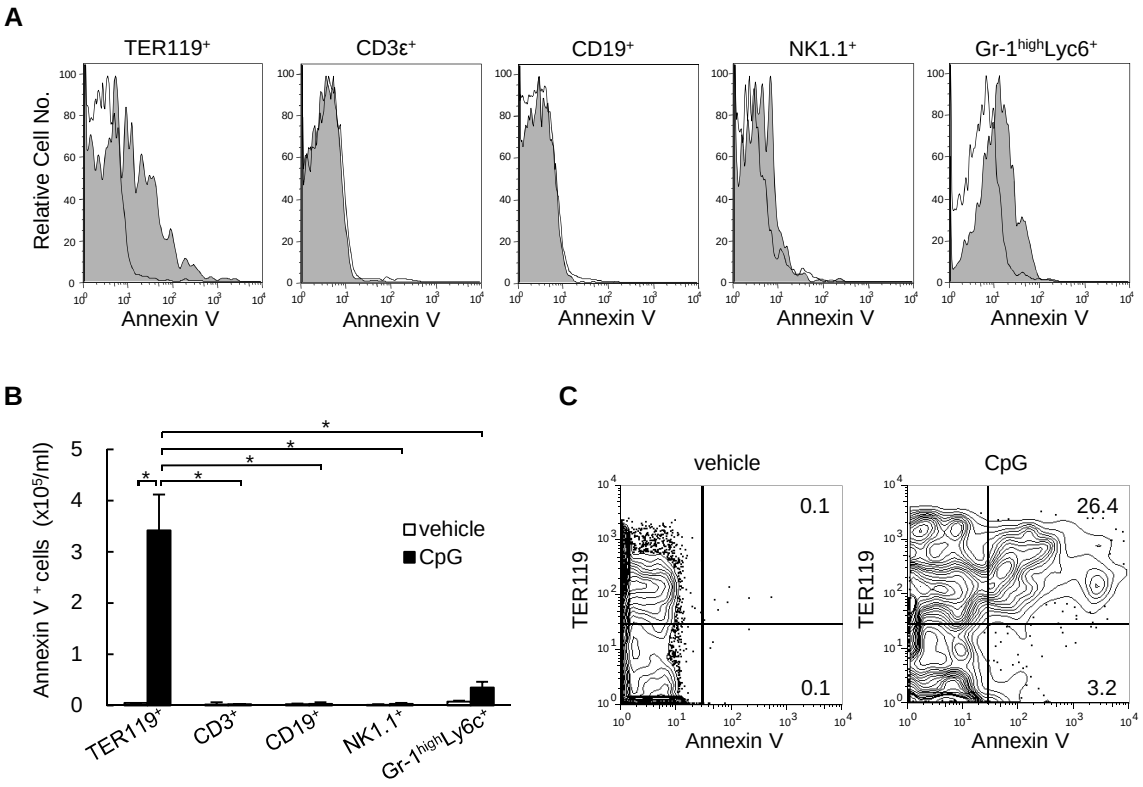

Figure S4. Apoptosis in CpG-injected WT mice.
(**A**) Representative FCM analysis of Annexin V staining in the different cell subset of the PB form WT mice 4h after PBS (open histogram) or CpG injection (shad histogram). (**B**,**C**) Absolute number of Annexin V$^+$ cells (**B**) and representative FCM analysis of Annexin V and TER119 staining (**C**) in the PB form WT mice 4h after PBS (vehicle) or CpG injection. Data represent the mean ± s.d. of three independent experiments. *P < 0.01.

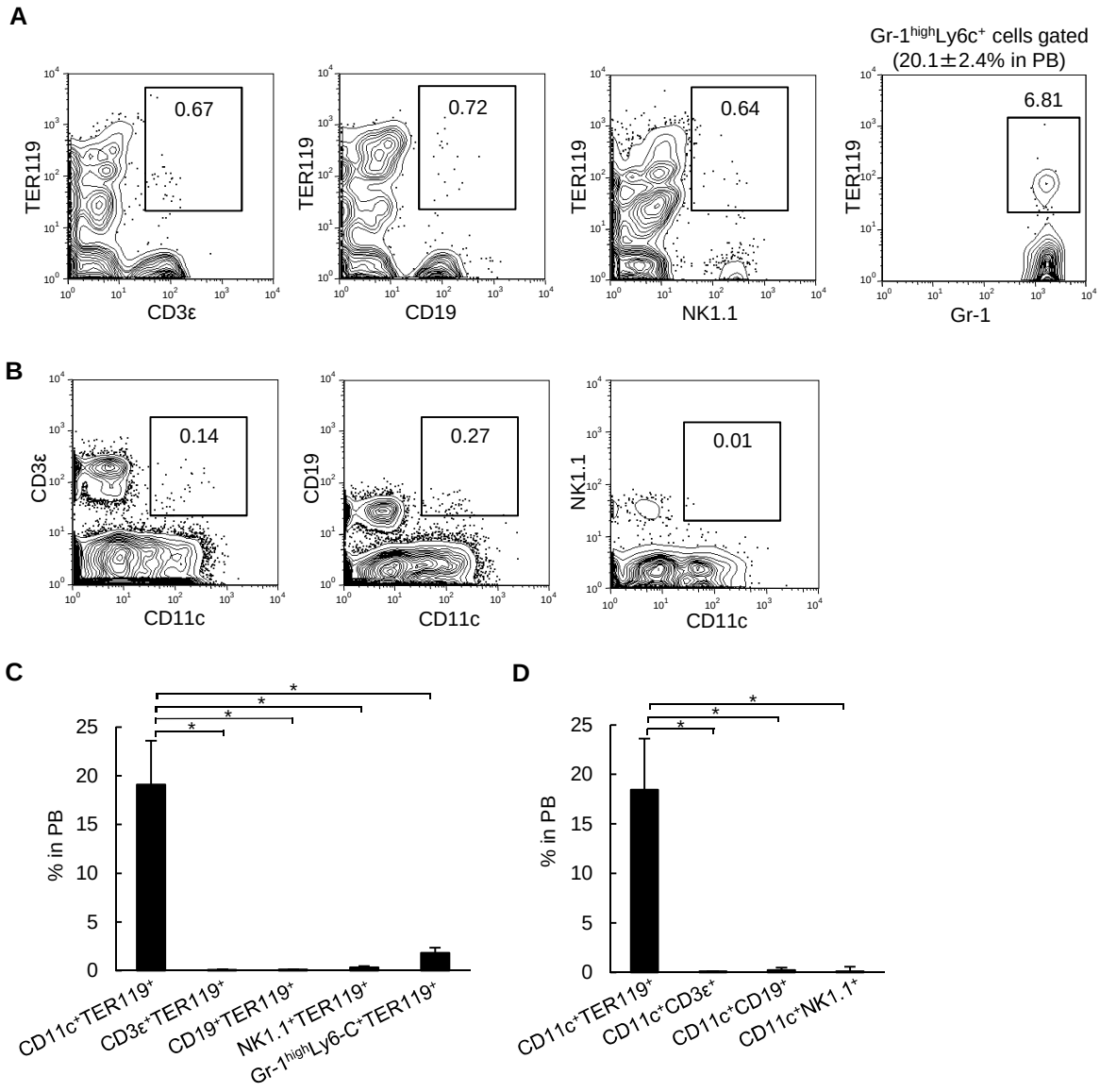

Figure S5. CD11c⁺ cells are the major phagocytes for TER119⁺ cells in the PB of Hemophagocytosis-induced mice. (**A**,**C**) Representative FCM analysis of the PB (**A**), and percentage of CD11c⁺TER119⁺, CD3ε⁺TER119⁺, CD19⁺TER119⁺, NK1.1⁺TER119⁺, and Gr-1^{high}Ly6c^{int}TER119⁺ cells in CpG-injected mice (**C**). (**B**,**D**) Representative FCM analysis of the PB (**B**), and percentage of CD11c⁺TER119⁺, CD11c⁺CD3ε⁺, CD11c⁺CD19⁺, and CD11c⁺NK1.1⁺ cells in CpG-injected mice (**D**). Data represent the mean ± s.d. of three independent experiments. **P* < 0.01.

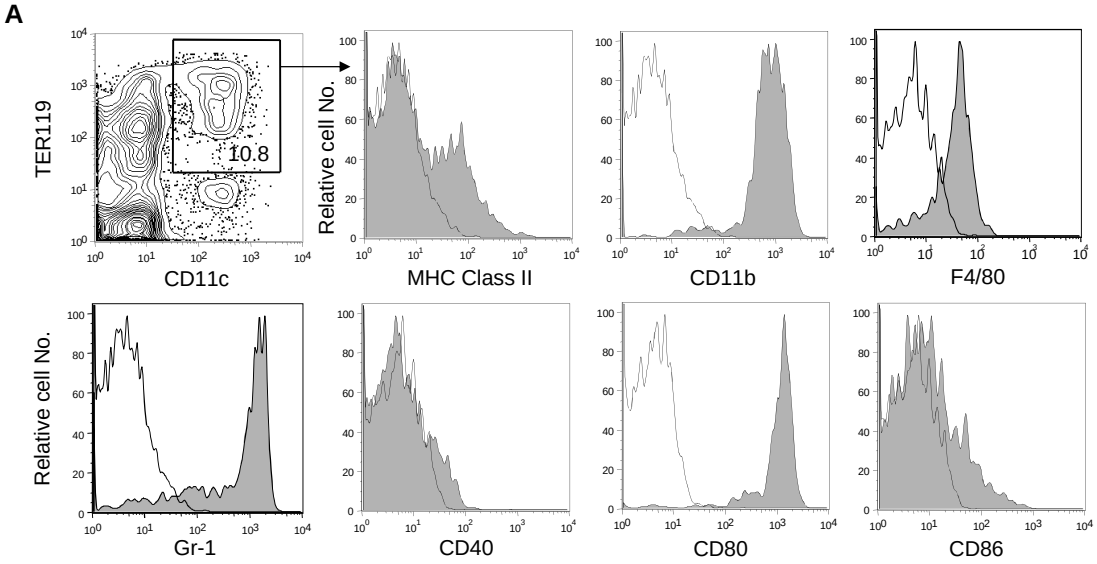
A
TER119
CD11c
10.8
Relative cell No.
MHC Class II
CD11b
F4/80
Gr-1
CD40
CD80
CD86

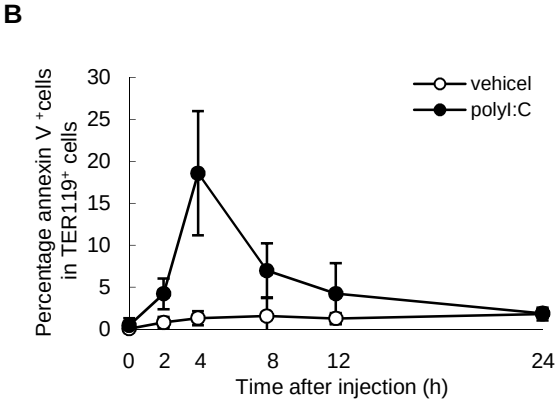
B
Percentage annexin V +cells in TER119+ cells
vehicel
polyI:C
Time after injection (h)

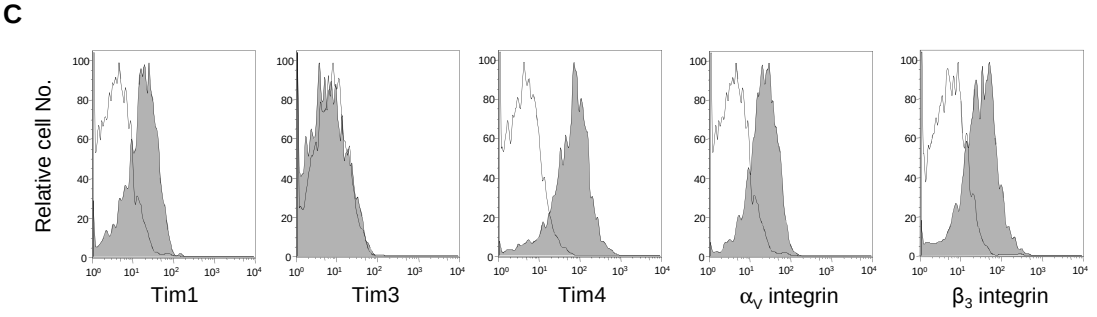
C
Relative cell No.
Tim1
Tim3
Tim4
αv integrin
β3 integrin

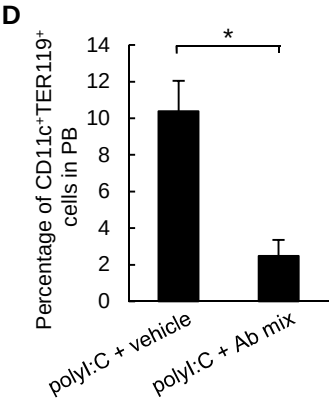
D
Percentage of CD11c+TER119+ cells in PB
polyI:C + vehicle
polyI:C + Ab mix

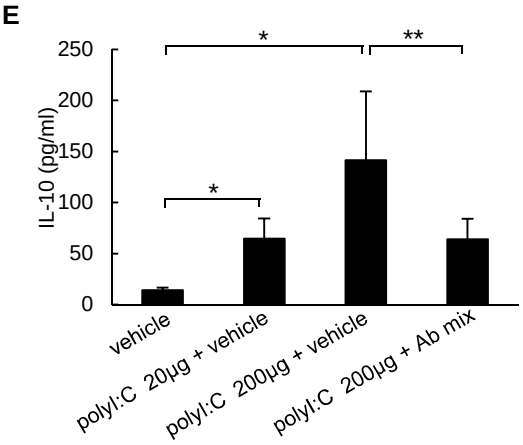
E
IL-10 (pg/ml)
vehicle
polyI:C 20μg + vehicle
polyI:C 200μg + vehicle
polyI:C 200μg + Ab mix

Figure S6. Mechanisms of poly I:C-induced hemophagocytosis.
(**A**) Phenotypic analysis of $CD11c^+TER119^+$ cells. $CD11c^+TER119^+$ cells gated on the contour plot were stained with mAbs to the indicated markers (shaded histograms) and isotype controls (open histograms). (**B**) Time course of the percentage of annexin V^+ cells among the $TER119^+$ cells in the PB of WT mice after PBS (vehicle) or 200-μg poly I:C injection. (**C**) Expression of "eat me" signal receptors on poly I:C-induced $CD11c^+TER119^+$ cells. Shaded histograms represent cells stained with mAbs specific for the indicated molecules, and open histograms show labeling with isotype controls. (**D**) Impaired poly I:C-induced hemophagocytosis in WT mice treated with neutralizing antibodies against Tim1, Tim4, α_V, and β_3. The proportion of $CD11c^+TER119^+$ cells 18 h after a 200-μg poly I:C injection together with a control rat IgG or with the indicated antibody mixtures (500 μg each). Ab mix, a mixture of antibodies against Tim1, Tim4, α_V, and β_3. (**E**) Serum IL-10 levels 24 hr after the indicated treatments. Data represent the mean ± s.d. of three independent experiments. $^*P < 0.01$. $^{**}P < 0.05$.

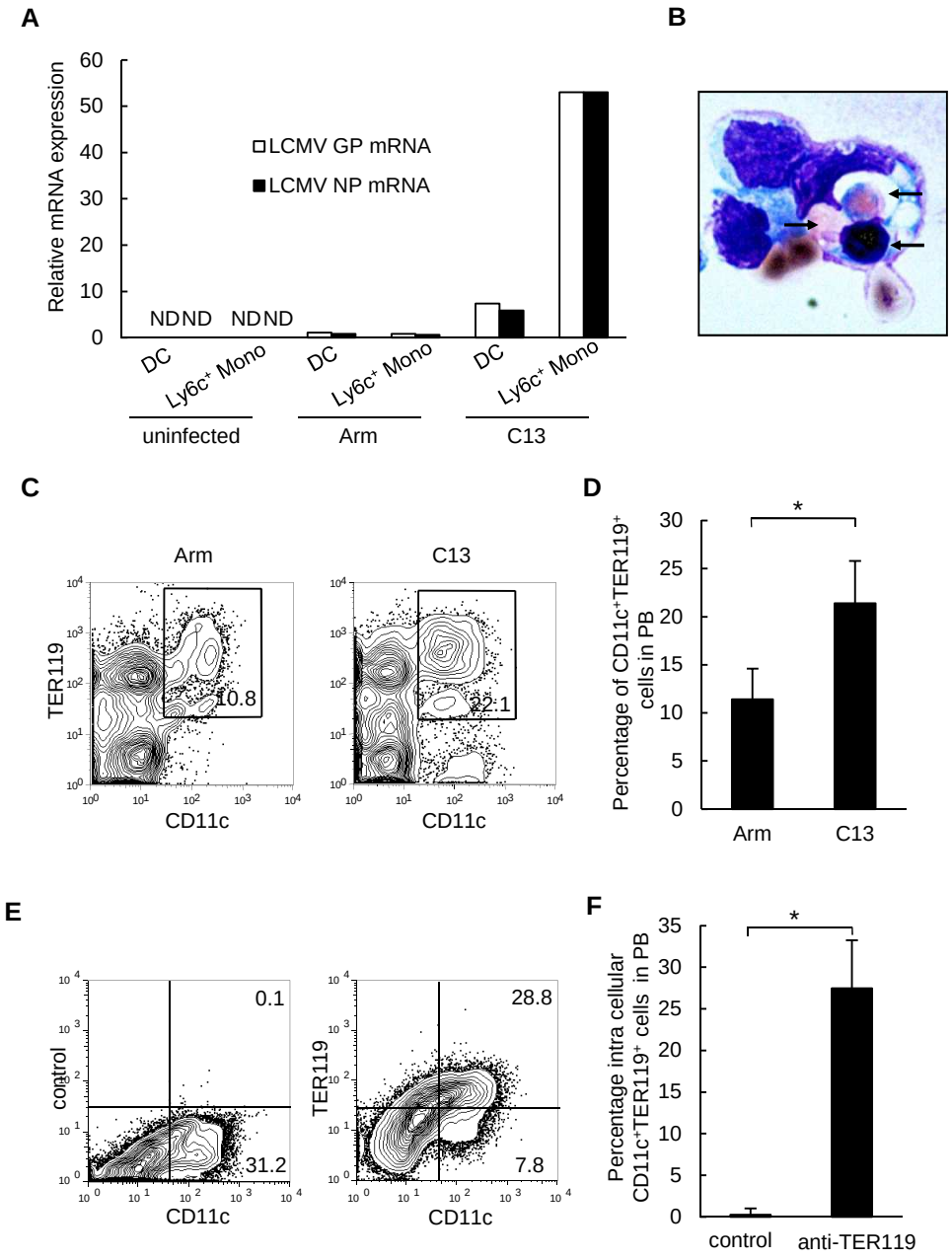

Figure S7. LCMV C13 induces efficient hemophagocytosis.
(**A**) Relative mRNA levels of LCMV glycoprotein (GP) and nucleoprotein (NP) in DCs (DC) and inflammatory monocytes (Ly6c$^+$ Mono) from WT mice 2 days after 2 x 10^6 pfu Arm or C13 infection. Cells were isolated from the BM of infected WT mice. Data are representative of three independent experiments. (**B**) Sorted CD11c$^+$TER119$^+$ cells from the BM of LCMV C13 infected mice were stained with Diff-Quick. Arrows indicate hemophagocytosed erythroid cells. Original magnification, x40. (**C**, **D**) Representative FCM profiles (**C**) and percentage (**D**) of CD11c$^+$TER119$^+$ cells in the PB of WT mice 24 h after 2 x 10^6 pfu Arm or C13 infection. Intracellular staining of TER119$^+$ cells inside CD11c$^+$ cells in mice infected with C13. (**E**,**F**) Representative FCM results (**E**), and percentage (**F**) of intracellular CD11c$^+$TER119$^+$ cells in the PB of WT mice 24 h after C13 infection. Data represent the mean ± s.d. of three independent experiments. *P < 0.01.

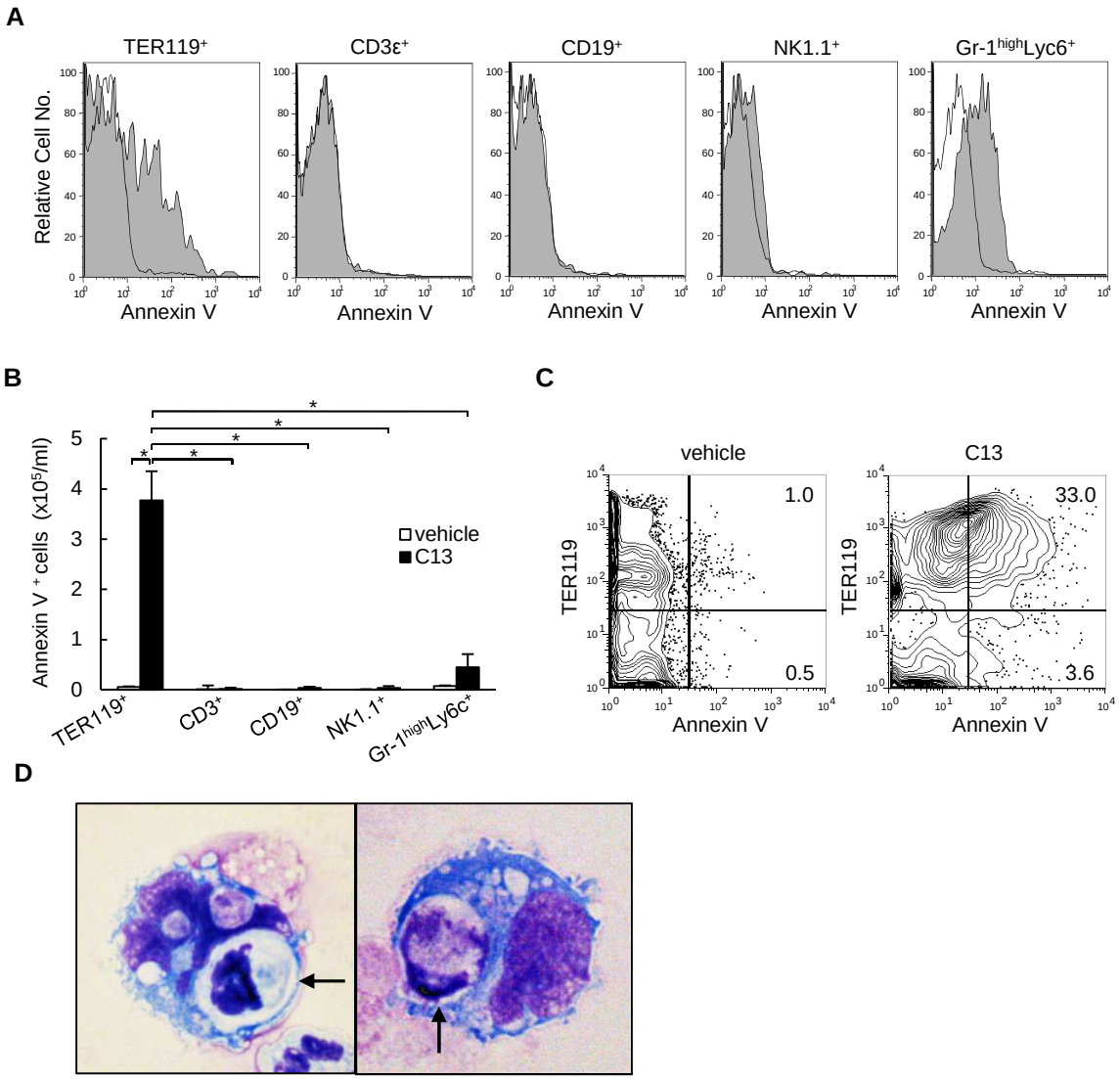

Figure S8. Apoptosis in LCMV C13-infected WT mice.
(**A**) Representative FCM analysis of Annexin V staining in the PB cell subsets form WT mice 4h after PBS (open histogram) or LCMV C13 infection (shad histogram). (**B**,**C**) Absolute number of Annexin V$^+$ cells (**B**) and representative FCM analysis of Annexin V and TER119 staining (**C**) in the PB form WT mice 4h after PBS injection (vehicle) or LCMV C13 (C13) infection. (**D**) Sorted hemophagocytes from PB of LCMV C13 infected WT mice, were stained with Diff-Quick. Arrows indicate hemophagocytosed granulocytes. Original magnification, x40. Data represent the mean ± s.d. of three independent experiments. *P < 0.01.

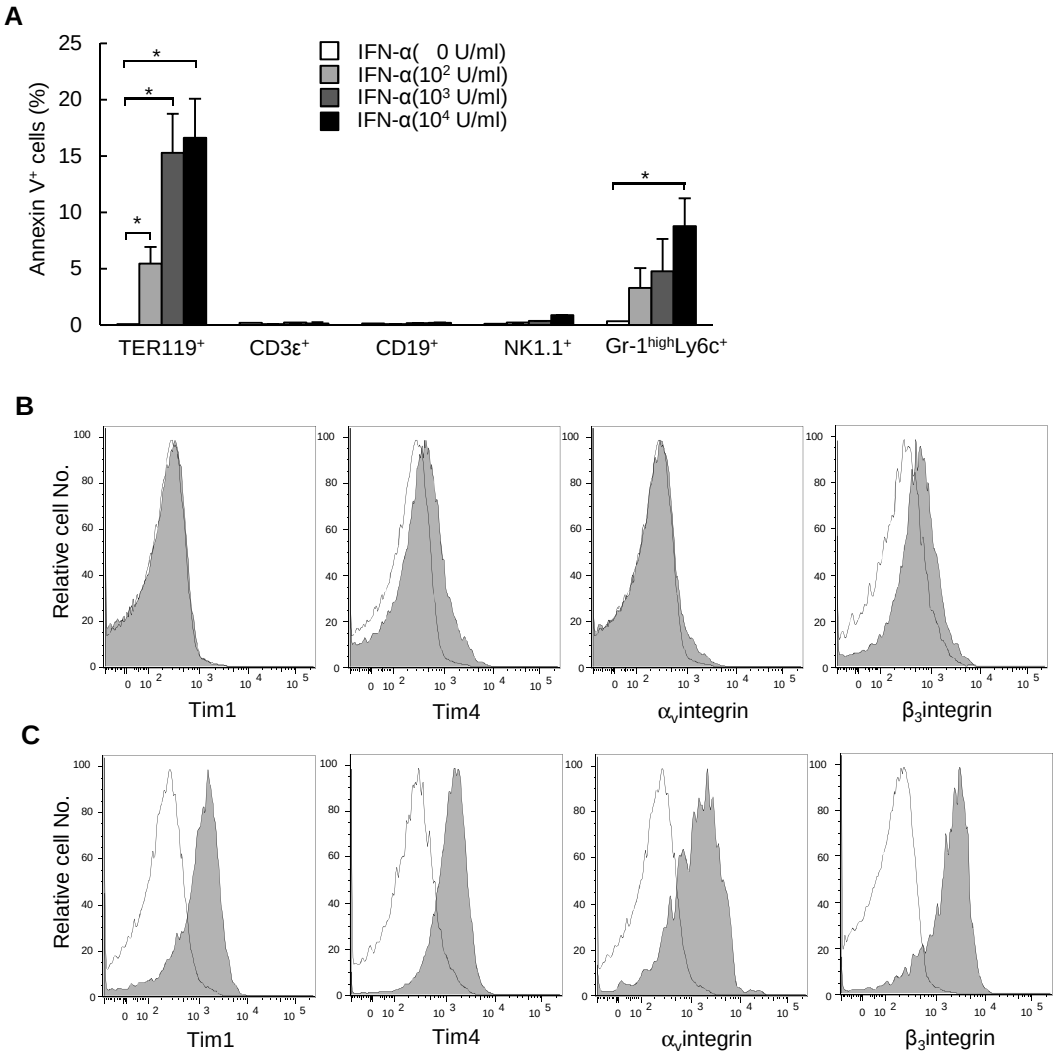

Figure S9. Interferon-α induces apoptosis and PS receptor expression in inflammatory monocytes.

(A) Percentage of annexin V⁺ cells in different cell type. Different cells from spleen of WT mice were stimulated with different concentration of interferon-α for 18h. Data represent the mean ± s.d. of three independent experiments. **P* < 0.01. (B,C) Representative FCM analysis of "eat me" signal receptors on inflammatory monocytes from BM of WT mice. Ly6c⁺ inflammatory monocytes were stimulated without (B) or with (C) interferon-α (10^4 U/ml) for 24h. One of representative data from two independent experiments.

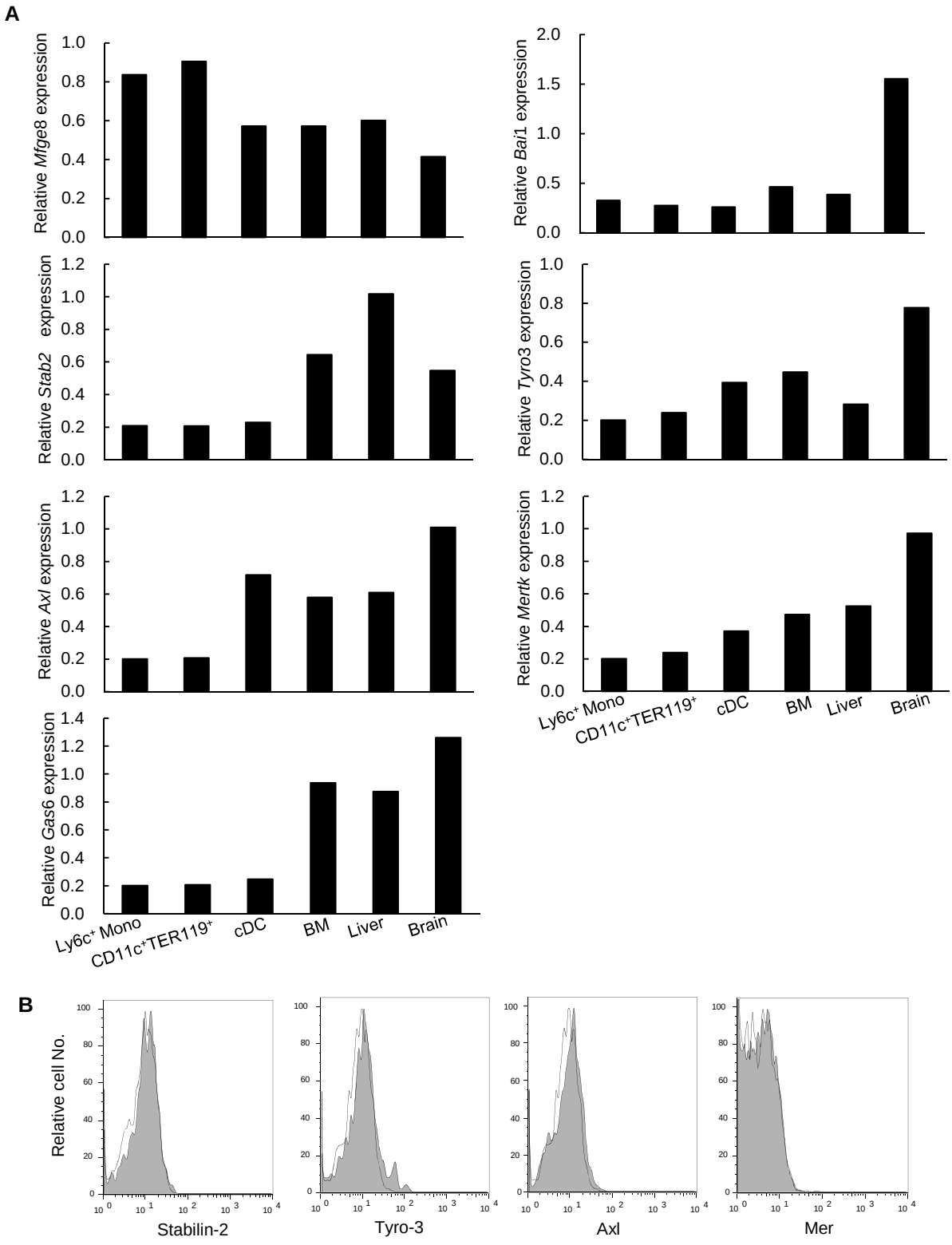

Figure S10. Expression of phosphatidylserine (PS) receptors and its recognition molecule in WT mice.

(**A**) Relative PS receptors and recognition moleculelel mRNA expression in the indicated cell populations and tissue from WT mice. cDC, conventional DC. (B) Expression of PS receptors on $CD11c^{+}TER119^{+}$ cells in the PB of WT mice 24 h after 2 x 10^{6} pfu C13 infection. Shaded histograms represent cells stained with Abs specific for the indicated molecules, and open histograms show labeling with isotype controls.

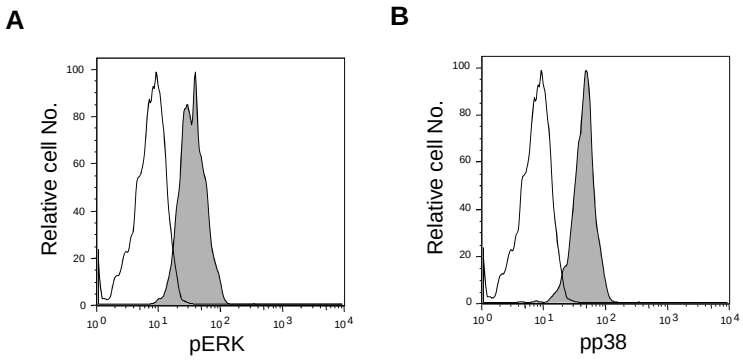

Figure S11. Phosphorylation of ERK and p38 in the hemophagocytosis-performing Mo-DCs of LCMV clone 13-infected WT mice. (**A, B**) PBMCs from WT mice 4 h after LCMV C13 infection were fixed with formaldehyde, permeabilized with methanol, and stained with cell-surface makers (CD11c and TER119), and pERK (**A**) or pp38 (**B**) (shaded histogram) and isotype control (open histogram). The data were gated on the $CD11c^{+}TER119^{+}$ cells. Data are representative of three independent experiments.

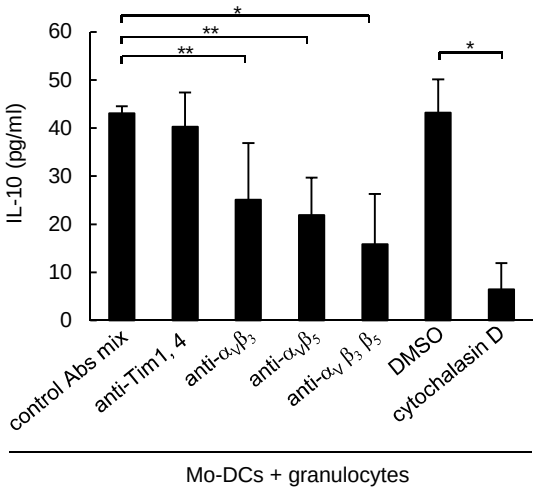

Figure S12. IL-10 production from Mo-DCs is dependent on hemophagocytosis. IL-10 level in the co-culture supernatants from the *ex vivo* hemophagocytosis assay. TER119$^-$ Mo-DCs and granulocytes from the BM of C13-infected mice were co-cultured with the indicated reagent(s) for 24 h. Data represent the mean ± s.d. of three independent experiments. *P < 0.01. **P<0.005.

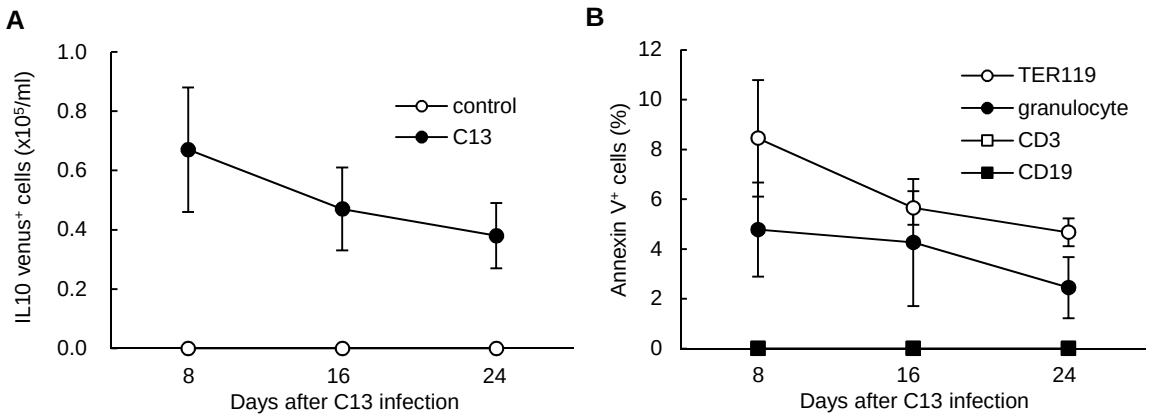

Figure S13. IL-10 production and apoptosis of TER119$^+$ cells and granulocytes are detected in the late phase of C13 infection.
(A) The absolute number of cells expressing IL-10 Venus in the Mo-DCs from the PB of *Il10*^{Venus} reporter mice after C13 infection. (**B**) Percentage of annexin V$^+$ cells in the indicated cells of PB of WT mice after C13 infection. Data represent the mean ± s.d. of three independent experiments.

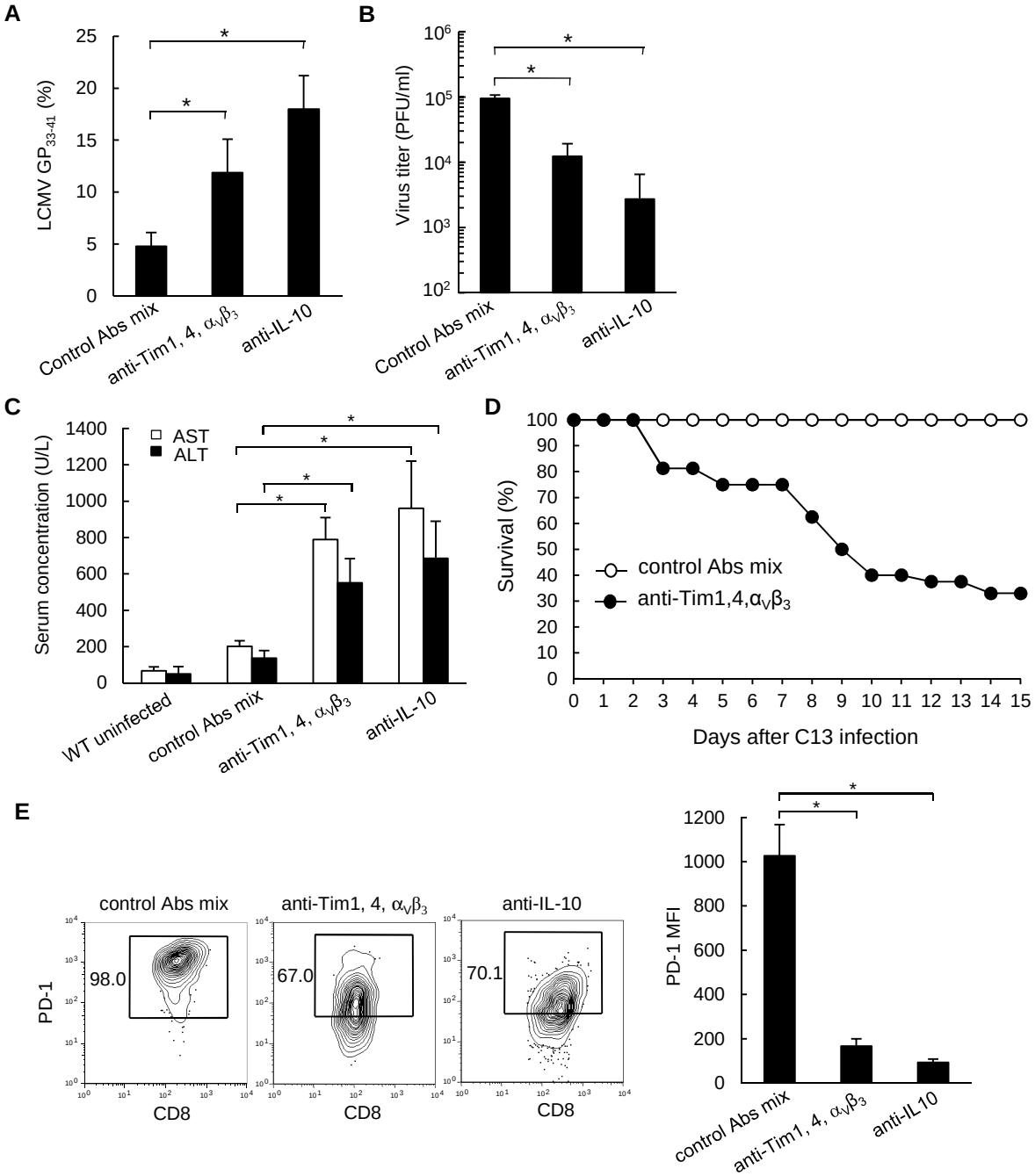

Figure S14. Altered immune responses in mice with limited hemophagocytosis and blocking of IL-10 production. (**A-C)** Percentage of LCMV GP_{33-41}-specific $CD8^+$ T cells in the spleen (**A**), titer of LCMV C13 in the serum (**B**), and level of AST/ALT in the serum (**C**) of uninfected WT mice and WT mice 9 days after LCMV C13 infection, with or without the injection of Abs to block PS receptors or neutralize IL-10. (**D**) Survival (%) of WT mice after LCMV C13 infection with or without the injection of Abs to block PS receptors. (**E**) FCM profile of PD-1 expression on LCMV GP_{33-41}-specific $CD8^+$ T cells in the spleen of WT mice 8 days after C13 infection, with or without injection of Abs to block PS receptors or IL-10-neutralizing Abs. MFI: mean fluoresce in intensity. Data represent the mean ± s.d. from three independent experiments. *P < 0.01.

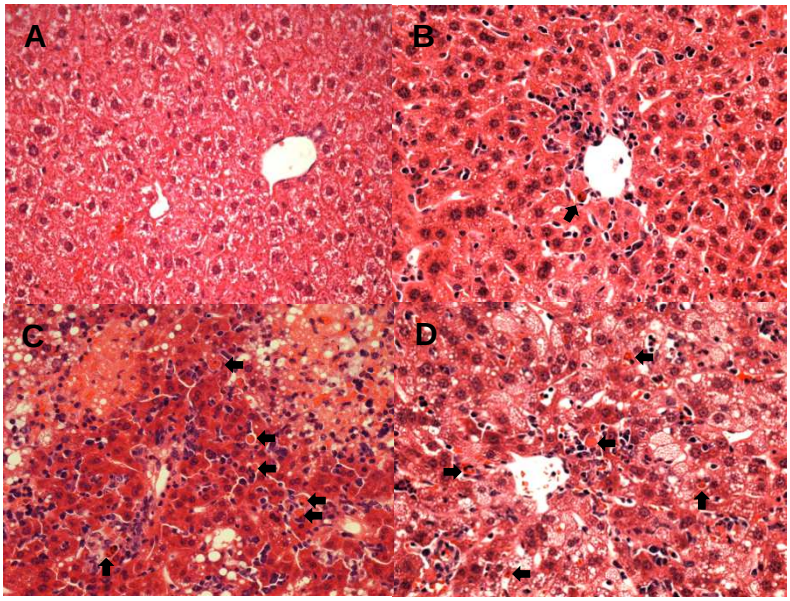

Figure S15. Inhibition of hemophagocytosis results in liver damage.
(**A-D**), HE staining of the liver from uninfected WT mice (**A**), WT mice infected with C13 (**B**), WT mice infected with C13 and treated with a mixture of antibodies against Tim1, Tim4, α_V, and β_3 (**C**), and WT mice infected with C13 and treated with anti-IL-10 Ab (**D**). Livers form C13-infected mice were prepared 9 days after infection. Many acidophilic bodies (apoptotic cells), indicated by arrows, are observed in (**C**) and (**D**). Data are representative from 5 mice. Original magnification, x 400.

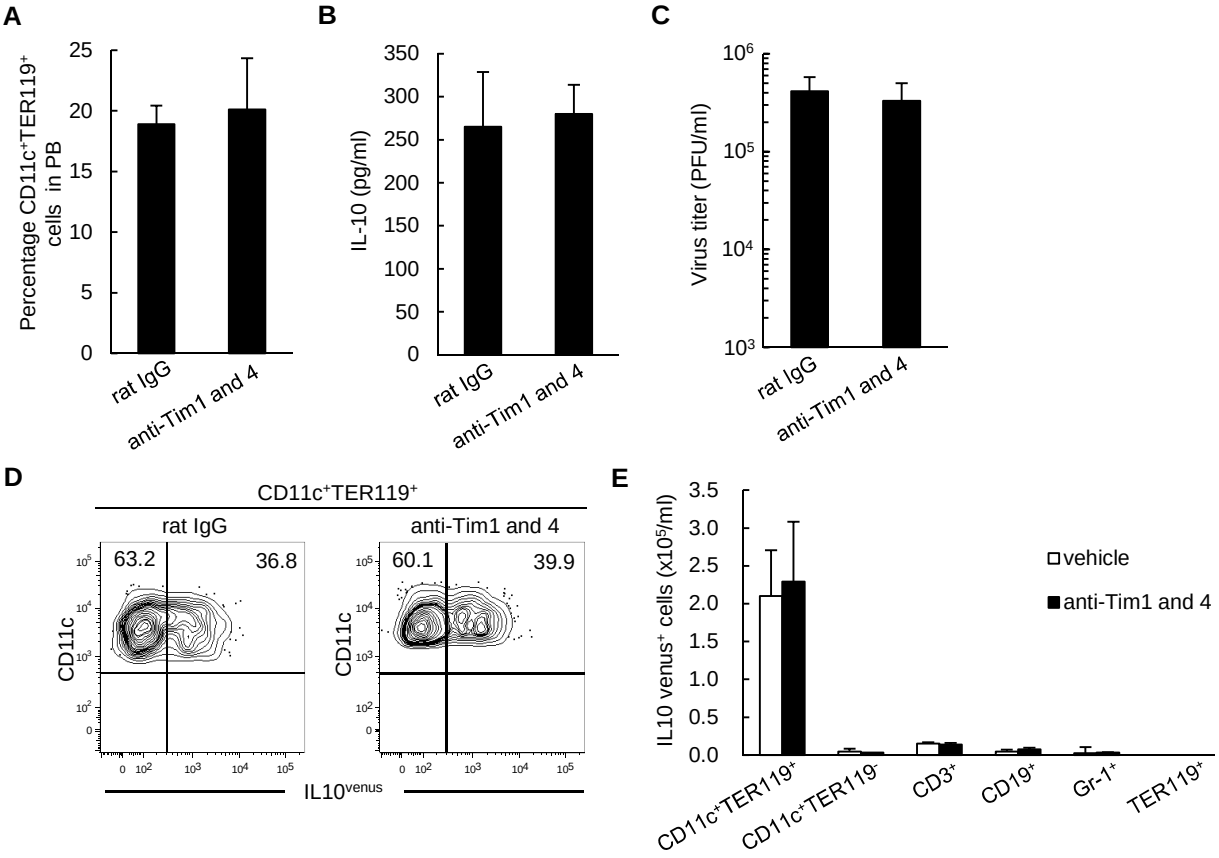

Figure S16. Administration of anti-Tim1 and 4 Abs does not alter immune responses in mice infected with LCMV C13. (**A-C**) Percentage of CD11c$^+$TER119$^+$ cells in the PB (**A**), IL-10 level (**B**), titer of LCMV C13 (**C**) in the serum of WT mice 9 days after LCMV C13 infection, with or without the injection of anti-Tim1 and 4 Abs. (**D**) A representative FCM profile of IL-10 Venus expression in CD11c$^+$TER119$^+$ cells from the PB of *Il10*^{Venus} reporter mice 24 h after C13 infection. (**E**) The cell number of IL-10 Venus$^+$ in the indicated cell populations from the PB of *Il10*^{Venus} reporter and WT mice 1 and 9 days after C13 infection. Data represent the mean ± s.d. from three independent experiments. *P < 0.01.

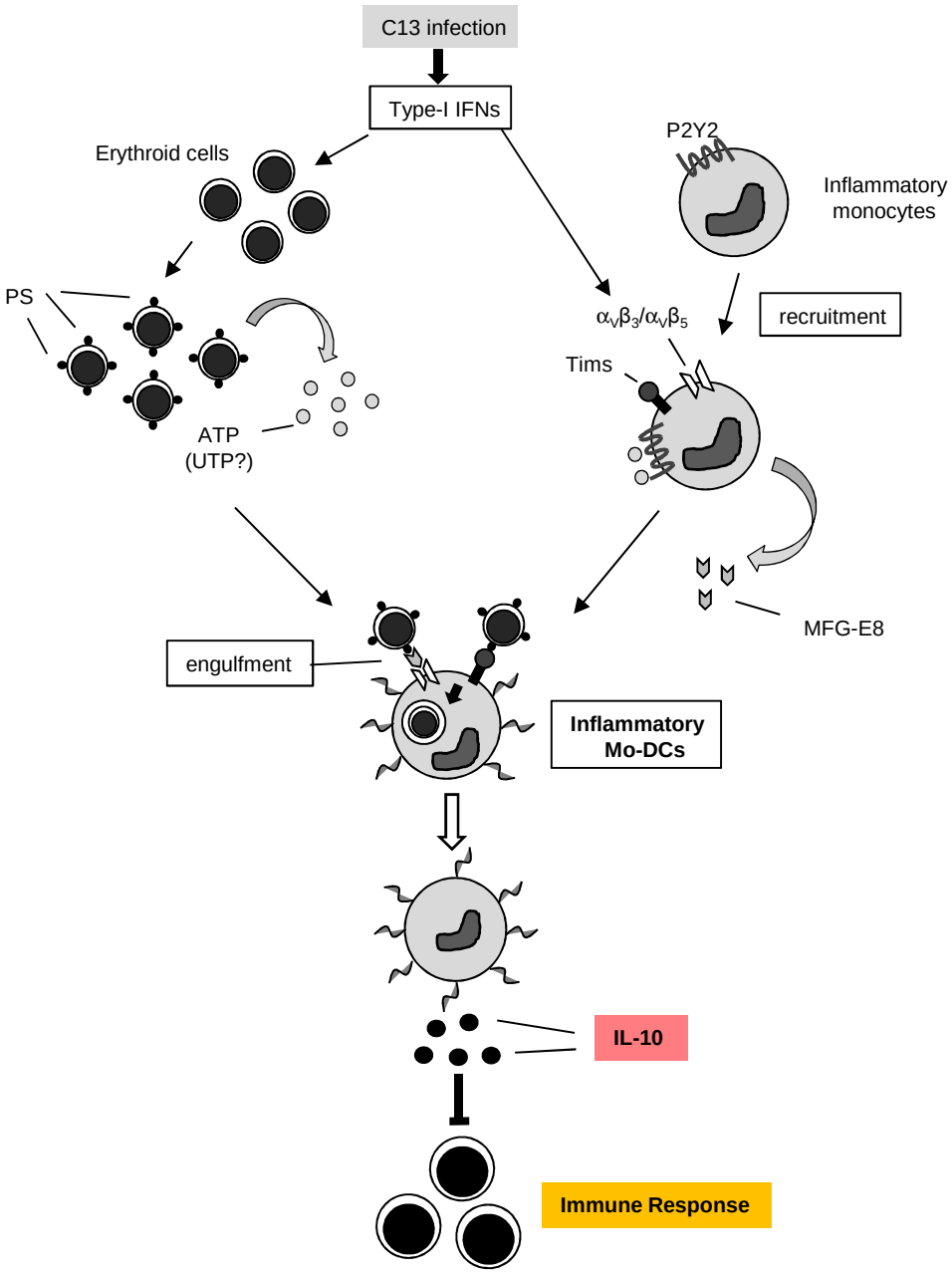

Figure S17. Schema of Hemophagocytosis development and Its Immunological Role.
Type I IFNs are produced immediately after C13 infection. The virus infection triggers both the activation of inflammatory monocytes and their differentiation into monocyte-derived dendritic cells (Mo-DCs), on which the cell-surface expression of phosphatidylserine (PS)-recognizing molecules ($\alpha_V\beta_3/\alpha_V\beta_5$ integrin, MFG-E8, and Tims) are upregulated; meanwhile, TER119$^+$ erythroid cells begin to expose PS on their surface as an “eat me” signal. Both events are induced in a type I IFN-dependent manner. Then, Mo-DCs perform hemophagocytosis and release an immunoregulatory cytokine, IL-10, to fine-tune the immune responses, including CTL activity.